J. Fluid Mech. (1985), *vol.* 158, *pp.* 399–446
Printed in Great Britain

Influence of rotation on the near-wake development behind an impulsively started circular cylinder

By MADELEINE COUTANCEAU
AND CHRISTIAN MÉNARD

Laboratoire de Mécanique des Fluides,† 40, Avenue du Recteur Pineau,
86022 Poitiers Cedex, France

(Received 5 January 1984 and in revised form 25 September 1984)

The early phase of the establishment of the flow past a circular cylinder started impulsively into rotation and translation is investigated by visualizing the flow patterns with solid tracers and by analysing qualitatively (flow topology) and quantitatively (velocity distributions and singular-point trajectories) the corresponding photographs. The range considered corresponds to moderate Reynolds numbers ($Re \leqslant 1000$). The rotating-to-translating-speed ratio α increases from 0 to 3.25 and the motion covers a period during which the cylinder translates 4.5 or even 7 times its diameter. The details of the mechanisms of the near-wake formation are considered in particular and the increase of the flow asymmetry with increase in rotation is pointed out. Thus the existence of two regimes has been confirmed with the creation or non-creation of alternate eddies after an initial one E_1. Furthermore, the new phenomena of saddle-point transposition and intermediate-eddy coalescence have been identified in the formation or shedding of respectively the odd and even subsequent eddies E_i ($i = 2, 3, \ldots$) when they exist. The very good agreement between these experimental data and the numerical results of Badr & Dennis (1985), obtained by solving the Navier–Stokes equations and presented in a parallel paper, confirms their respective validity and permits the determination of the flow characteristics not accessible, or accessible only with difficulty, to the present experiments. These flow properties such as drag and vorticity are capable of providing information on the Magnus effect for the former property and on unsteady separated flows for the latter.

1. Introduction

It is well known that a rotating body, travelling through a fluid in such a way that the rotation axis is at right angles to the translational path, experiences a transverse force, called generally the Magnus force after the German physicist who first investigated it experimentally in 1853. In the present study the body is a cylinder of radius R rotating about its axis with angular speed ω_0 and translating with a uniform velocity V_0 or, what is equivalent in a frame accompanying the cylinder in its translation, a rotating cylinder placed in a uniform stream V_0. In this case the existence of a lift force may be explained easily from the theory of inviscid fluids (Batchelor 1967). It is induced by the asymmetry of the two flows on each side of the cylinder: the speed on the part of the cylinder that moves in the direction of the free stream is higher than that on the other side, which moves against the free stream,

† Laboratoire associé au C.N.R.S. dans le cadre du L.A. n° 191.

giving rise to asymmetrical pressure distributions produced by the Bernoulli effect and consequently to a transverse force towards the high-velocity side. The corresponding lift coefficient is found to increase in direct proportion to the peripheral-to-translating-speed ratio α ($=\omega_0 R/V_0$).

In a real fluid, the phenomenon also exists and is equally important but the evolution of the Magnus lift with α appears to be not so simple. In particular, because of viscous effects which induce the development of a boundary layer along the cylinder surface and its possible separation, the Reynolds number Re ($=2V_0R/\nu$) appears as another relevant parameter. The flow depends also on other parameters such as surface conditions, aspect ratio, end shapes, wall confinement. So, taking into account the possible applications, for example in ballistics and wind propulsion, many measurements were made in the first part of the century to evaluate the influence of the various parameters. These studies, which concerned high Reynolds numbers ($Re > 5000$), are reviewed, with the more recent ones (Charrier 1979; Calamote 1984), in the thesis of Ménard (1984). The results appeared to be particularly sensitive to the effects of aspect ratio and so it was necessary for experimenters to investigate the best manner to approximate the two-dimensional flow. These precautions being taken, it was found that for low speed ratios ($\alpha < 1$) the lift coefficient increases regularly with α up to Re of about 5×10^4. But, beyond this, a minimum is encountered; this minimum increases with Re and even becomes of opposite sign (Magnus-effect paradox) for $10^5 < Re < 5\times10^5$ and α decreasing from 0.45 to 0.17. From $\alpha = 1$, the lift coefficient becomes independent of the Reynolds number; the corresponding curve is a regularly increasing function of α, but with a decreasing slope from α of about 3. A qualitative explanation of the experimental observations was proposed by Krhan (1955) and Swanson (1961) by means of a global analysis of the boundary-layer behaviour and its separation. In particular they introduced the interesting notion of two relative Reynolds numbers to take into account the difference existing on each side of the cylinder between the relative velocities of the wall compared with that of the free stream and consequently the difference in the initiation of the turbulence. But, for a complete explanation of the motion, the nature of the wake should also be considered. It appears that there is a lack of detailed information concerning this. However, from the visualizations of Prandtl (Prandtl & Tietjens 1934) for $Re \approx 4000$ and α up to 6 and from the very recent ones of Calamote (1984) for $1000 < Re < 8000$ and α up to 8, it seems that, for low values of α, eddies would be alternately shed on each side of the cylinder to form a Bénard–Kármán street, as for the pure translation ($\alpha = 0$). But the eddies on the side moving in the direction of the rotation decrease progressively when α increases and then disappear completely. Thus it was found that the Bénard–Kármán structure begins to deteriorate as soon as the peripheral velocity becomes greater than the free-stream velocity (giving rise to a zigzag oscillating wake) and finally disappears for $\alpha \gtrsim 2.5$.† Then the two boundary layers meet and vorticity is swept downstream in a sort of 'plume' as described by Calamote (1984). An analogous result was obtained for $Re = 9000$ by Diaz *et al.* (1983) by a spectral analysis of the velocities measured with hot probes in the relatively near wake.

The phenomena appear to be very complex and strongly dependent on the speed ratio α and so it would be interesting to be able to predict them. But, up to now, no theoretical formulation has been able to do this in a general way. The first attempt

† This is also in agreement with the visualizations obtained by Werlé about twenty years ago for $Re \cong 3300$ and recently reported in Werlé (1984).

at obtaining an analytical representation was made by Bickley (1928) who took the vorticity shed in the wake into account by superposing a vortex in the neighbourhood of the cylinder on the potential flow with circulation. Then an extension of this technique was proposed by Gustafson (1933), replacing the single vortex by a set of vortices of constant intensity and introducing the Oseen approximation. Somewhat later other studies were made on the basis of boundary-layer theory such as those of Glauert (1957*a*,*b*), Moore (1957) and Wood (1957) from which an increasing lift coefficient with α may be deduced. But they are limited to very small or high speed ratios and cannot relate the wake formation and the separation phenomena. More recently, owing to the availability of computer studies, new data have been provided by Ta Phuoc Loc (1975), Townsend (1980) and Ingham (1983) from solving numerically the Navier–Stokes equations, the only ones capable of giving complete information relative to the whole flow field. However the solution procedure raises numerous difficulties, as mentioned by Ta Phuoc Loc (1975), in particular because of poor convergence. So these studies were limited to small Reynolds numbers; the two first authors considered the cases $Re = 5$ and 20 and α up to 0.5 and the third $Re = 5$, 20, 30 and α up to 5; all three authors used the steady-state equations. Although some discrepancies appear in their results, it may be deduced that rotation delays and may even inhibit the boundary-layer separation. Thus at $Re = 30$, whereas for $\alpha = 0$ the recirculating zone is well developed (its length is about 1.5 times the cylinder diameter), no eddies were detected by Townsend (1980) in the established wake for $\alpha > 1$. Data relative to the aerodynamic coefficients are also given, showing that the Magnus effect exists even for these low Reynolds numbers. But, again, discrepancies and even contradictions appear in their conclusions for the evolution with α. The experimental data available to support the validity of the calculations appears to be still more scarce than for high Reynolds numbers. In particular, except for the photographs of Prandtl (Prandtl & Tietjens 1934) that are open to criticism because they were taken on a free surface, only a few other flow visualizations have been published, by Taneda (1977, 1980) (for $Re = 100$; $\alpha = 1.73$ and $Re = 49$; $\alpha = 0.63$) and by Koromilas & Telionis (1980) (for $Re = 50$ and $\alpha = 0.8$). But the latter investigations were made in general studies relative to unsteady laminar-flow separation† and the corresponding photographs are proposed only as examples among many others. Consequently, no systematic study of the flow structure and of the influence of each of the significant parameters, viz Reynolds numbers, speed ratio and time, has been made and no quantitative data were deduced. However some confirmation of the observations of Prandtl was provided and some precise details given. Thus Koromilas & Telionis (1980) gave details of the saddle-point patterns near the downstream- and upstream-moving parts of the wall. Taneda compared the visualizations obtained with the aluminium-dust technique (giving streamlines) and with electrolytic precipitation on the whole surface of the cylinder (giving streaklines). He showed that, under the experimental conditions, dye is shed from a unique point of this surface, whereas two eddies are apparent in the streamline pattern. This shedding point is located upstream on the side that moves against the rotation.

These results are very interesting, but they remain fragmentary. So, in concert with Badr & Dennis (1985), it was decided to extend and complement the previous studies by considering, numerically for Badr & Dennis and experimentally in the present work, the case when the cylinder is set impulsively into rotation and translation in

† Taneda (1977) considered the time development of the flow about a cylinder impulsively started either into rotation and translation or only into rotation in a uniform stream, whereas Taneda (1980) and Koromilas & Telionis (1980) examined the case of the established regime.

order to study the flow development with time. The object of the present investigation is to obtain both qualitative and quantitative experimental information on the flow structure and velocity fields sufficiently precisely to detect the details of the process of the near-wake formation and to serve as a guide for the calculations. Since the numerical scheme can be adapted to correlate with the experiments and can be completely controlled, all the characteristics may then be deduced, including those which are not accessible or only studied with difficulty in the experiments. Thus, by means of this collaboration, a complete and reliable study may be undertaken.

The notation and definition of the significant parameters are the following:

$$\text{Reynolds number:} \quad Re = \frac{2V_0 R}{\nu};$$

$$\text{peripheral-to-free-stream-speed ratio:} \quad \alpha = \frac{\omega_0 R}{V_0};$$

$$\text{scaled time:} \quad t^* = \frac{tV_0}{2R};$$

so that the cylinder translates a distance equal to its diameter during the unit scaled time.

In the experiments α is varied between 0 and 3.25, the range in which, as appears from the previous data given in the literature, the main different structures are liable to occur. Three values of the Reynolds number were selected, $Re = 200$, 500, 1000; the case $Re = 200$ will serve as a reference and will be discussed in detail in this paper. The period of observation is limited, because of the apparatus, to $t^* = 4.5$ or 7 at best. The calculations of Badr & Dennis (1985) cover precisely the same range of parameters except that they are restricted to $\alpha = \frac{1}{2}$ and 1. It is therefore possible to correlate exactly our experimental results with these calculations. Their most detailed calculations are given for $Re = 200$ and we have found almost exact agreement with their results in this case for every measured property of the solutions, not merely qualitatively but also quantitatively, as can be seen from the paper by Badr & Dennis.

2. Experimental technique

2.1. *The presentation*

The experimental technique is essentially the same as that previously used and described by Coutanceau & Bouard (1977*a*) and Bouard & Coutanceau (1980) for investigating the time development of the flow structure around an impulsively started translating cylinder. It is based on visualization of the flow pattern by means of solid tracers and on a detailed analysis of the corresponding photographs to determine the important points (stagnation points, centre of the vortices, etc.) and also the measurement of some velocity profiles. Thus the information we are able to deduce from our experiments is effectively sufficiently precise to serve as a guide for detailed comparison with, and even improvement of, numerical techniques. This has been clearly illustrated, in particular, in the calculations of Ta Phuoc Loc (1980) and Rinaldo & Giorgini (1983).

In the present work, the flow is produced by causing the cylinder, rotating about its horizontal axis, to rise vertically along the median plane of a tank of rectangular cross-section filled with a quiescent liquid. The rotation is generated from the

translation through a mechanical device and the camera accompanies the cylinder in its translation. The visualization is achieved by illuminating, along a thin plane of the cylinder cross-section, solid tracers uniformly put in suspension in the fluid and by taking photographs with a suitable exposure time. Thus it is possible to visualize in a translating frame of reference the precise situation of the numerical calculations, which are performed in a similar frame.

Schematic illustrations of the apparatus are given in figures 1(*a*) and (*b*). An elevating carrier supports both the camera and a frame on which is fixed the cylinder and the device which induces the rotation. This carrier is translated upwards by a system of pulleys and balance-weights; its speed is regulated by a dash-pot below the camera. The rotation is induced from the translation by means of pinions and cog belts (figure 1*b*): the start of the carrier causes the driving pinion (i) to rotate via the cog belt (iii) attached to a fixed point. The speed of rotation can be imposed by selecting a reducing gear (ii).

In the present experiments the speed of translation varies between 0.5 and 5 cm/s and the rotation-to-translation-speed ratio ranges from 0 to about 3.5. To obtain a good definition of the flow pattern cylinders with diameters of 4 and 6 cm were selected. In fact, the 6 cm one was more often used, the smaller one being used essentially to extend the scaled time of observation and to establish some comparisons in order to evaluate the wall effects. The tank in which the experiments are carried out is 46×56 cm in cross-section and 100 cm in height. The cylinder moves midway between the walls which are farthest apart and, to minimize end effects, the clearance between the extremities of the cylinder and the two other tank walls was made as small as possible, so that the aspect ratio of the cylinder is either 7.3 or 11.2. The translational displacement of the cylinder is limited to 30 cm by the length of the regulating dash-pot.

Once the diameter of the cylinder and the range of its translation speed have been imposed, the liquid contained in the tank is chosen according to the selected range of Reynolds numbers. In the present work two different mixtures of paraffin oil with a suitable solvent (having kinematic viscosities respectively of 6.5 and 4.5 cm^2/s) were used for $Re = 200$ and 500 and water for $Re = 1000$. The photographs are taken after given intervals of time following the start of the motion, i.e. after distances covered by the cylinder which correspond to the selected values of t^*. One photograph only is taken for each experiment. In order to minimize the bottom and free-surface effects, this photograph is taken about 35 cm before the cylinder reaches the free surface; the height at which the motion must be started is determined from the value of t^*.

It has been verified that the start of the translational motion is quasi-instantaneous; it is demonstrated in the thesis of Ménard (1984) that the limiting velocity is reached in less than 0.1 s. This has been controlled by means of an optical device associated with a microprocessor. In addition, the device inducing the rotation synchronizes the translational and rotational motion and they start simultaneously and, because of the use of the cog belts, no slip can occur. Other details, such as those concerning the lighting device, the choice of the visualization particles and the measurement of the translation speed, may be found in Coutanceau & Bouard (1977*a*) and Bouard & Coutanceau (1980) and in the thesis of Bouard (1983); the system of rotation is presented in the thesis of Ménard (1984).

The principle of the analysis of the photographs is the same as that described by Coutanceau & Bouard (1977*a*) but using the more effective apparatus described by Ménard (1984). It permits the precise location of the characteristic flow points and of the extremities of the dashes described by the tracers during the time of exposure.

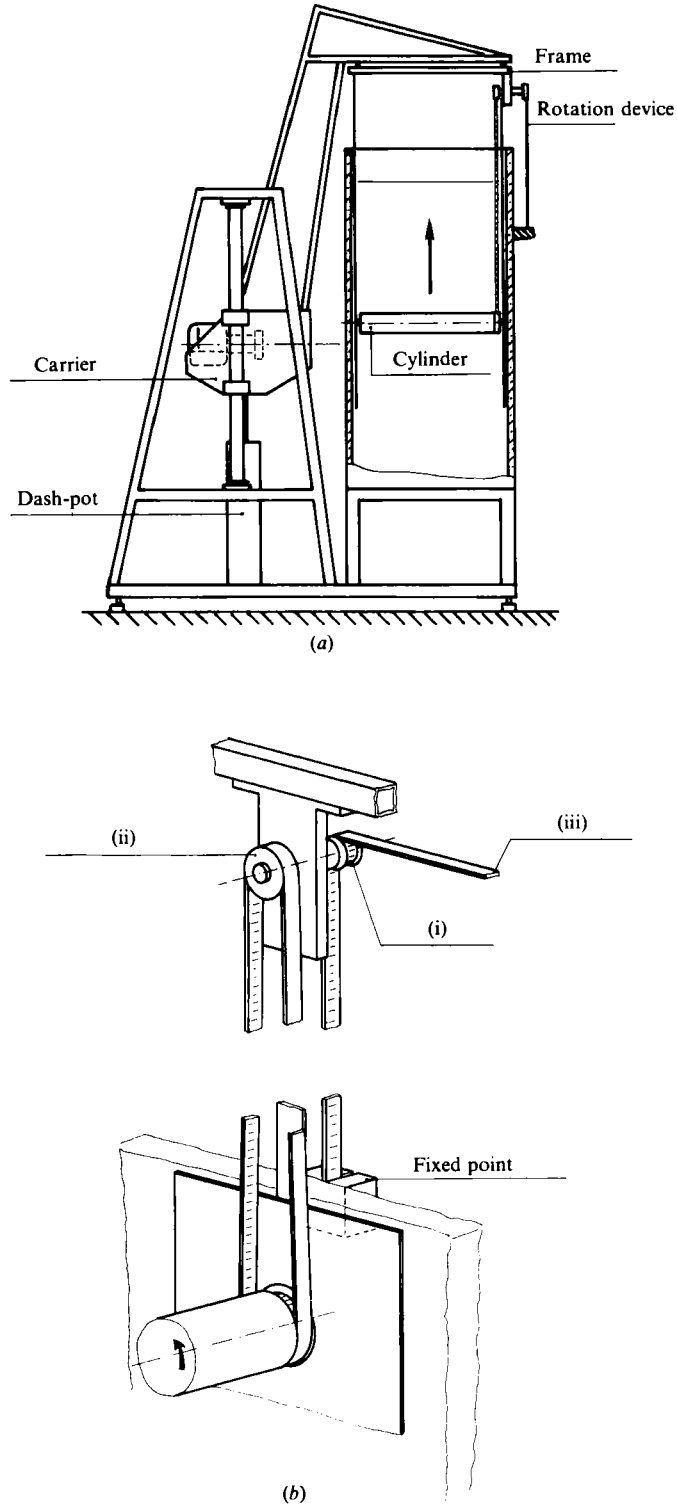

FIGURE 1. Schematic illustration of the experimental apparatus: (*a*) general view; (*b*) detail of the system of rotation.

This location is made to within 0.05 mm directly on the enlarged ($\times 4$) negative films (9×12 cm^2). Thus precise values of the velocities may be obtained; it is often accurate to within 5%. However, since this location determination remains manual, the velocity distributions have been determined only along the two flow axes. Furthermore, to supplement the photographs and give a precise determination of the flow structure, construction of the streamline patterns has also been undertaken with a special effort to determine the singular ones that pass through the various stagnation points. This construction has been made directly by projecting the films onto an enlarger. (It is not possible to determine the streamlines from the measured velocities by calculation since these velocities are known only along the two axes of the flow field.) It may be that under these conditions it is not possible to obtain exact streamlines. However the excellent agreement with the corresponding numerical results of Badr & Dennis (1985) proves that this difficult work (it is often difficult to decide if fluid is inside or outside an eddy) has been done with care and discernment. In fact, these line drawings of the flow pattern have constituted a valuable guide for the calculations, indicating the zone to explore in more detail.

2.2. *Some comments*

In addition to the previous comment in relation to the validity of the proposed streamline patterns, other points are open to question. For example the experimental flow cannot be exactly two-dimensional everywhere, in particular because of the end-effects. Furthermore, since the flow is unsteady, the white dashes of the photographs do not represent exactly parts of streamlines, but parts of trajectories. But, once more, confirmation is given by comparison with the numerical results of Badr & Dennis (1985). The agreement is equally good for the streamline patterns as for the velocity profiles and singular point trajectories. Thus it is clear that the aspect ratio of the cylinder is sufficient for the flow to be quasi-two-dimensional, at least in its median part, and that three-dimensional instabilities have no time to appear during the initial phase considered in this work, except for $Re = 1000$ and the greatest values of α for which three-dimensional phenomena have been observed. Likewise, the sidewalls have no appreciable effects, except for the largest values of α and for large times (Ménard 1984), and the time of exposure has been chosen to be sufficiently short for the white traces left by the particles on the photographs to represent effectively quasi-instantaneous-velocity vectors giving, by visual integration, streamline patterns.

Thus it appears that our experimental technique is effectively very well adapted to the determination of these characteristics. It is also likely that other features would be interesting to predict, such as the aerodynamic coefficients needed to study the establishment of the Magnus effect and the vorticity for help in understanding the unsteady separation phenomena. However, their evaluation would be very difficult with our apparatus and not precise. So, this complementary information is given by the numerical calculations of Badr & Dennis (1985), as explained in the introduction.

3. Some general points on the flow topology and notation

Before discussing the structure of the flow pattern revealed by the visualization photographs, we will outline some general points and the notation. Compared with the well-known case of pure translation (i.e. $\alpha = 0$), special features occur due to the fact that the rotation of the cylinder destroys the symmetry of the flow, at least in

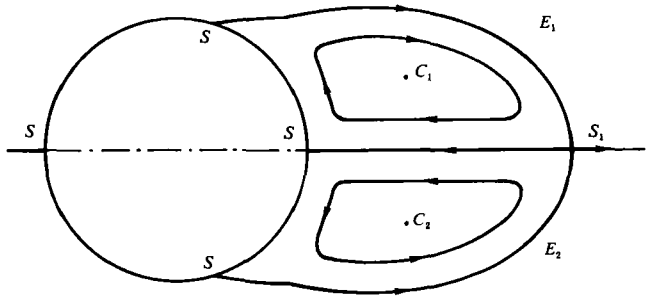

FIGURE 2. Instantaneous configuration of the recirculating zone that takes place, during the early phase of flow development, behind a cylinder started impulsively into a pure translation.

its neighbourhood, and that the wall is in motion in relation to the camera. So, to point out more clearly these features, we will first recall the main characteristics of the flow when Re is several hundred and $\alpha = 0$.

Since the fluid is considered to be incompressible, the start of the translation of the cylinder instantaneously generates a motion in the fluid which is irrotational everywhere. But then, because of the relative velocity of the fluid and solid boundary, vorticity is generated from the wall and is progressively transported by diffusion and convection instream (for these Re, convection plays the major role in the near wake), very rapidly inducing separation of the flow and the formation of a closed recirculating zone. In this case ($\alpha = 0$), because of the symmetry of the velocity gradient, this zone is made up of two opposed symmetrical eddies E_1 and E_2, figure 2. The upper one rotates clockwise, whereas the lower one rotates anticlockwise; they have a common boundary SS_1. (Bouard & Coutanceau (1980) show that in the period of the flow establishment secondary eddies also appear near the separation point when $Re > 500$.) The recirculating zone grows in width and length with time, while remaining for a certain period of time ($t^* < t_L^*$) symmetrical and stably attached to the cylinder. After this the eddies become asymmetrical and are shed alternately downstream to form the so-called Bénard–Kármán street. From the results of Honji & Taneda (1969) one may deduce, for example, that for $Re = 200$ (our reference value) t_L^* is about 8. So, for this value of the Reynolds number and during the period considered in the present work, which extends up to 7 at the most, the recirculating zone (when $\alpha = 0$) remains symmetrical and attached to the cylinder. Thus, as is shown in figure 2, two types of stagnation point may be distinguished: those (S) located on the stationary body wall, including the front and the rear stagnation points and the two separation points, and that (S_1) located at the end of the closed wake corresponding to the intersection of the two branches of the streamline that enclose the two eddies. Such a branching point is generally called a saddle point and corresponds to an 'instream' stagnation point where the flow configuration is of the type shown on figure 3(a). In this particular case of $\alpha = 0$, because of the symmetry of the closed wake, the vorticity is zero at this point and consequently the two branches of the streamline intersect at a right angle: thus there is an orthogonal saddle point. But, as was mentioned by O'Brien (1981), the non-orthogonal saddle-point configuration (figure 3b) can also exist and is even more widespread. Indeed, this is effectively the configuration that we shall encounter in the flow induced by a rotating and translating cylinder, both at the front stagnation point and at the 'closure' point of the eddies.

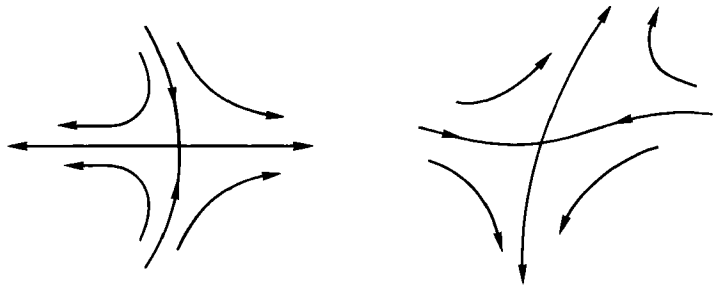

FIGURE 3. Examples of streamline saddle-point configurations: (*a*) orthogonal configuration; (*b*) non-orthogonal configuration.

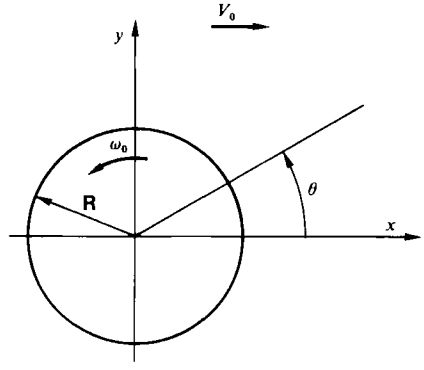

FIGURE 4. The reference frame.

Let us consider now precisely what happens when $\alpha \neq 0$, i.e. when a rotation is superposed on the translation with reference to the same previously discussed translating frame; the rotation is assumed to be anticlockwise as indicated on figure 4. Thus, at the start of the motion, the flow is the same as for $\alpha = 0$, as will be verified by means of the time evolution of the velocity profiles, but, as soon as viscosity effects occur, differences in the flow appear. First, the wall shear gradient becomes asymmetrical since the upper side of the cylinder moves against the free stream whereas the lower side moves in the direction of the free stream. Thus, at $t^* = 0$, the relative velocities of the fluid compared with that of the wall are respectively $(2+\alpha)\,V_0$ and $(2-\alpha)\,V_0$ for $\theta = \pm 90°$; compared with the free stream these wall relative velocities becomes $(1 \pm \alpha)\,V_0$. Consequently, the symmetry of the wall vorticity is destroyed and the flow separation induces asymmetrical eddies, arising earlier on the upper side of the cylinder than on the lower side. This phenomenon becomes much more marked as the relative rotation (i.e. α) increases; the lower eddy appears later and becomes weaker and smaller, completely disappearing when α exceeds about 2. This may be connected with the fact that under these conditions, in the lower part of the flow, the maximum of the initial-stream-to-wall relative velocity vanishes for $\alpha = 2$ and changes sign for $\alpha > 2$. Then the wall does not continue to reduce the fluid velocity but, on the contrary, accelerates it.

Another difference compared with the $\alpha = 0$ case is due to the motion of the

cylinder wall relative to the frame of observation. Hence, immediately after the start of the motion, a thin fluid layer rotates with the cylinder and stagnation points can no longer lie on the cylinder wall; they must occur in the fluid itself. In particular, this is true for the front stagnation point from which the flow divides to pass around the obstacle; let us call this point S. It will be seen that it is established rapidly at its definite location in the upper upstream quarter of the flow where it has moved against the direction of rotation. We should note that the movement and final position of this stagnation point will be found to agree with the calculations of Badr & Dennis (1985). Furthermore, as was mentioned above, depending upon the value of α, other instream stagnation points may appear in conjunction with the creation of eddies. Let us call these eddies E_i, where i indicate their order of detachment, and C_i and S_i respectively their centres and closure saddle points. In certain cases, two intermediate eddies will coalesce to form a single final one: we call them E_i' and E_i''. Thus E_3' and E_3'' coalesce to form E_3.

As examples figures 5 (a) and (b) present two typical sketches for low values of α. The first shows the flow just after the start of motion: two asymmetrical eddies are formed. It may be noticed that, contrary to the $\alpha = 0$ case, they have no longer a common boundary but are separated by fluid that passes around them and, because of their respective rotation, they 'close' in opposite directions: E_1 closes towards downstream in S_1, whereas E_2 closes towards the cylinder wall in S_2. These eddies grow with time in size and strength as more and more fluid passes between them. However, during the initial phase, they almost accompany the cylinder in its translation as if they were attached. But the upper eddy E_1, developing more rapidly, is then shed downstream. Then E_2 continues to develop with its closure point S_2 moving up along this rotating layer until it is shed in its turn, initiating the Bénard–Kármán-street process. Then, as suggested in figure 5 (b), E_2 moves away from the cylinder, whereas two intermediate clockwise eddies E_3' and E_3'' respectively appear in the upper and lower part of the very near wake; afterwards, they will progressively move towards each other before finally combining to form E_3.

At this stage, it is interesting to recall that from Taneda's (1977, 1980) visualizations it is seen that when $Re = 49$ and $\alpha = 0.63$ dye is shed only from a unique point on the upstream side of the cylinder moving against the free stream (the upper side for us) as if the two previous separation points of figure 2 have merged towards the front stagnation point, which itself has moved counter to the sense of the rotation. Thus it may be thought that, in the near wake and in analogous experimental conditions, vorticity convection would play the essential role in the upper-wake side, whereas vorticity would be transported by cross-diffusion in the lower part of the flow.

Finally, before closing this section on the general presentation of flow structure, a few comments must be made about the recirculating fluid cells which form in the wake of the cylinder, which we call eddies in preference to vortices, to avoid the confusion with vorticity, which has a local significance. Furthermore, although the term of vortex shedding is of general use in fluid mechanics, some uncertainty remains in the definition of vortices in unsteady flows. For example Mehta (1975) used the term vortex to define closed equivorticity lines, whereas the definition proposed by Lugt (1979) is based on closed or spiralling pathlines viewed in an appropriate frame assuring the flow to be quasi-steady. Thus it seems that no different terminologies have been imposed to designate what is 'pictured' respectively in instantaneous streamline patterns (with small tracers) and streakline patterns (with smoke or dye), perhaps because this second process has been the most often used for visualizing unsteady flows. However, as mentioned by Perry, Chong & Tim (1982),

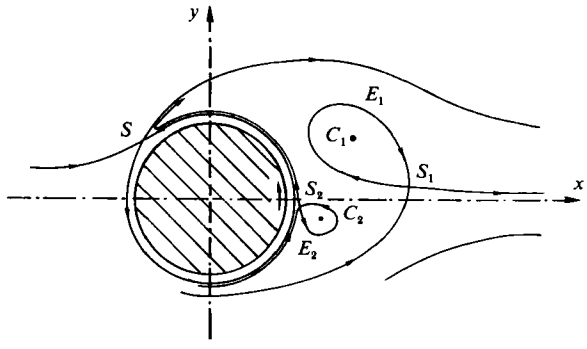

(*a*)

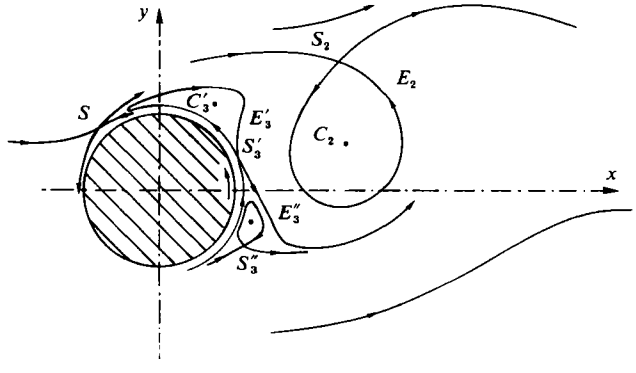

(*b*)

FIGURE 5. Configuration of the streamline pattern around a rotating and translating cylinder for small values of α: (*a*) configuration of E_1 and E_2 during the initial phase; (*b*) configuration of E_3' and E_3'' just before their combination.

the relation between instantaneous streamlines and streaklines is extremely complex. Indeed, smoke and dye give an idea where the vorticity resides but tell us very little about the surrounding field and do not provide quantitative information, whereas instantaneous flow pictures with small particles do not permit us to follow precisely the spreading of vorticity but may be used to deduce quantitative information about the velocity fields and consequently constitute precise means for comparison with numerical calculations. It is with this object that we use this last technique. It should be recalled also that, since the streamlines are not invariant with respect to the motion of the reference frame, the loop of the singular streamline that bounds an eddy, when it resides immediately behind the body, where velocities are low, decreases and even is transformed into a wave (the centre and the closure saddle point of the eddy move towards each other before finally merging), when this eddy is shed within the fluid. This is because of its downstream motion relative to the cylinder centre (thus relative to the camera) and because of the diffusion of its vorticity. In this range of Re, diffusion plays a lesser role in the mechanism of eddy decrease. As mentioned by

Lugt (1979), to follow correctly the development of an eddy, the observer should move with its centre.

Having now given sufficient information about the object of the present work, the possibilities and the limitation of our experimental technique and our notation, we will describe our visualization photographs and discuss some of the curves deduced from them. Because of the complete lack of previous theoretical or numerical data, comparisons will be established only with those of Badr & Dennis (1985); these numerical results will be presented, so that they can be used to support the experimental observations, in their complementary paper.

4. Time development of the wake flow pattern for $Re = 200$ and $\alpha = 0.5$

In the first instance we will describe the time evolution of the wake for $Re = 200$, the reference value, and $\alpha = 0.5$; i.e. the speed of the cylinder wall is half the translation speed. The wake flow pattern is presented both on the photographs of figure 6, which show quasi-instantaneous-velocity fields (the non-dimensional time of exposure being less than 0.1) for scaled time t^* regularly increasing from 0 to 6.5 by steps of $\Delta t^* = 0.5$ and $\Delta t^* = 0.25$ for the earlier phase where the flow structure evolves more quickly, and on the streamline patterns (figure 7). At time $t^* = 0.5$, when the cylinder has just had time to translate a distance of only half its diameter, the upper eddy E_1 may be suspected to have formed already. At $t^* = 0.75$ it is well formed and simultaneously, on the lower side, there appears a bulge in the streamlines, indicating a reduction of the velocity of the fluid particles passing through this region and announcing the birth of E_2. This second eddy E_2 is indeed visible at $t^* = 1$. Then the two saddle points S_1 and S_2, closing E_1 and E_2 respectively, are in opposite directions as has been described in the previous section. It is seen also that S_1 is only slightly above the longitudinal x-axis and S_2 below it. As t^* continues to increase to 2, E_1 and E_2 grow, and their respective centres C_1 and C_2 move away from the cylinder; C_1 travels a little more rapidly than C_2. During this period, the saddle points S_1 and S_2 remain on opposite sides of the x-axis: S_2 goes up towards the x-axis, while S_1 remains at an approximately constant distance from it.

For $t^* > 2$, new phenomena begin to appear. First, E_1 becomes stretched towards the downstream direction, giving to the zone which is next to the front stagnation point S an elongated shape like a tongue. Secondly, the growing and the swelling of E_2 cause its saddle point S_2 to rise along the rotating layer and to cross the x-axis, swept along by the rotation. Since the displacement of S_2 is greater than the corresponding displacement of the centre C_2, the distortion of the streamlines existing in the region below S_2 increases and forms a 'fluid wedge' which the fluid particles enter before turning back. These phenomena are clearly visible for $t^* = 2.5$. In addition, from this time S_1 begins to move up away from the x-axis, indicating the onset of the shedding of E_1 into the general stream. At $t^* = 3$ E_1 is clearly shed and it starts to decrease. Then, for $t^* = 3.5$, a new phase commences with the rapid development of E_2 causing the 'fluid wedge' to be more accentuated and the 'fluid tongue' to split away from the rest of the fluid surrounding E_2. The separation of this part of the fluid gives rise to a new eddy E_3'; the corresponding saddle point S_3' is in the downstream direction above E_2 (figure 6*h*). At $t^* = 4$ E_2 has grown considerably and exhibits almost circular streamlines; its size is then a maximum. One also notices that, at this stage, S_2 has abruptly moved up onto the upper part of E_2. In fact S_2 now approximately takes the place of S_3', while S_3' has gone downwards almost to where S_2 was; so there is in this sense a transposition between

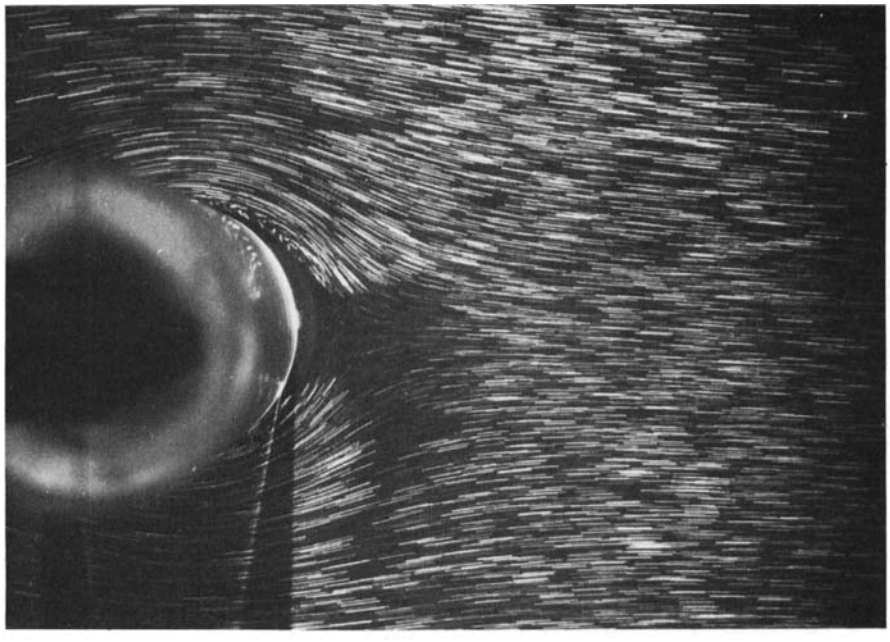

(*a*) $t^* = 0.5$

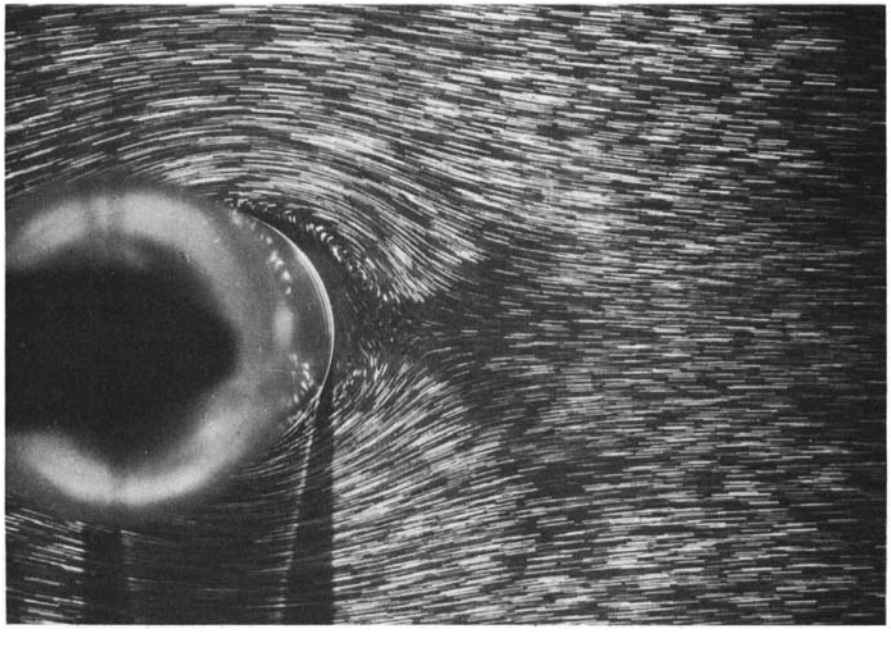

(*b*) $t^* = 0.75$

FIGURE 6(*a*,*b*). For caption see page 417.

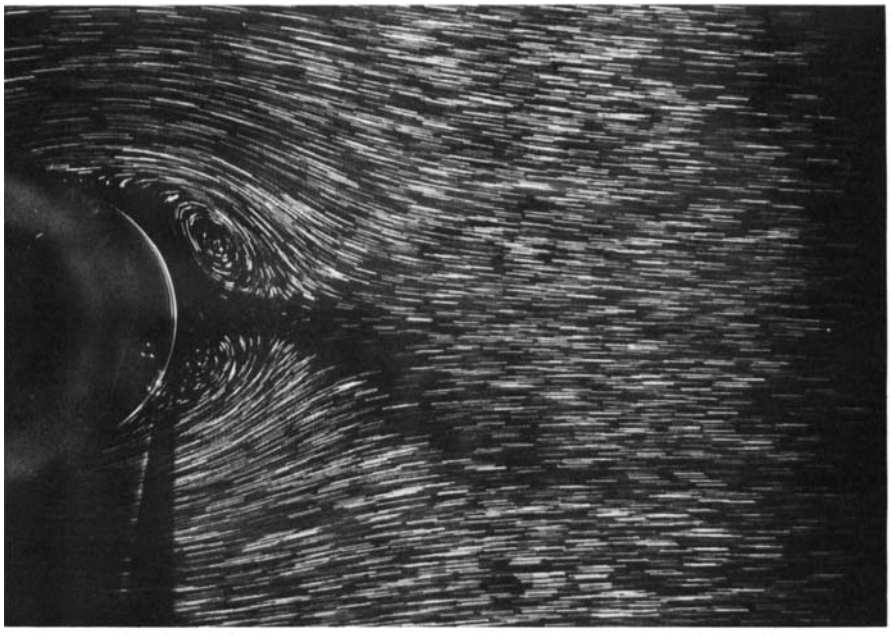

(*c*) $t^* = 1$

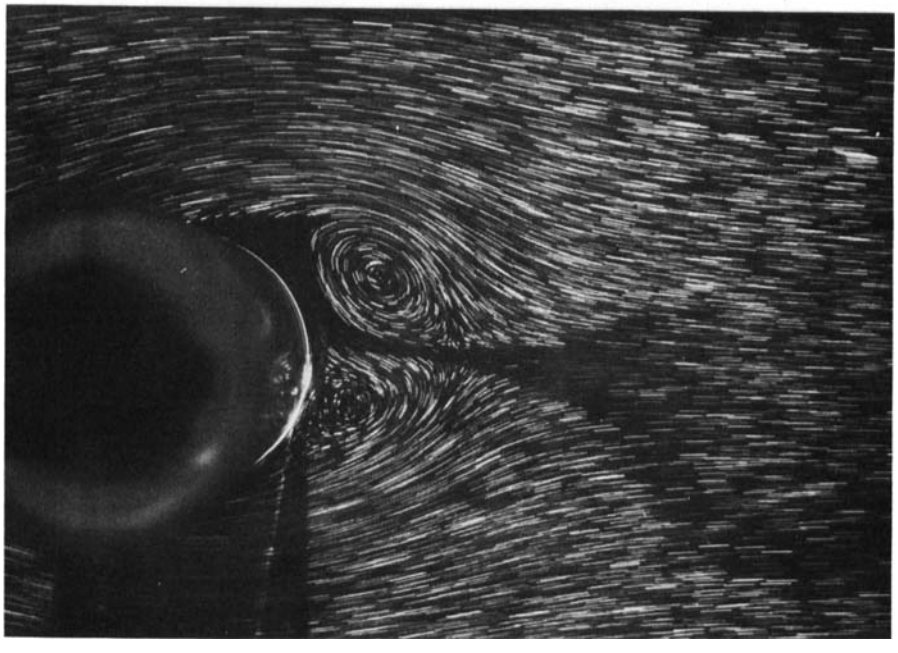

(*d*) $t^* = 1.5$

FIGURE 6(*c*,*d*). For caption see page 417.

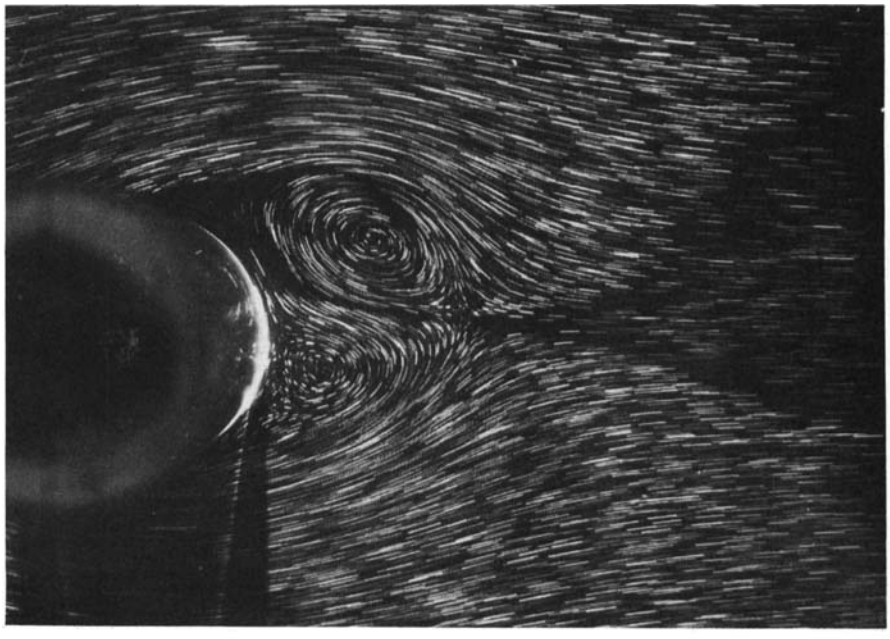

(*e*) $t^* = 2$

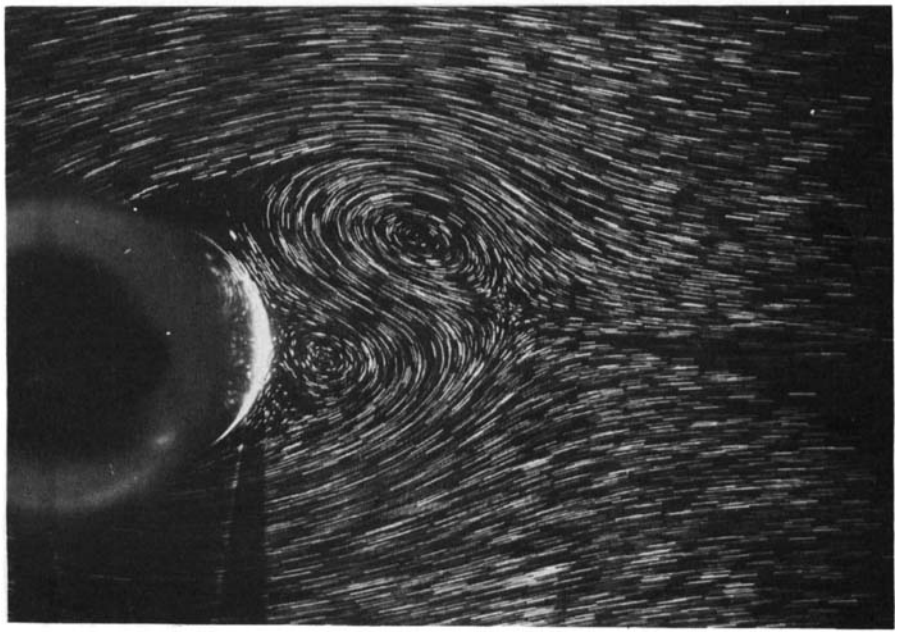

(*f*) $t^* = 2.5$

FIGURE 6(*e*, *f*). For caption see page 417.

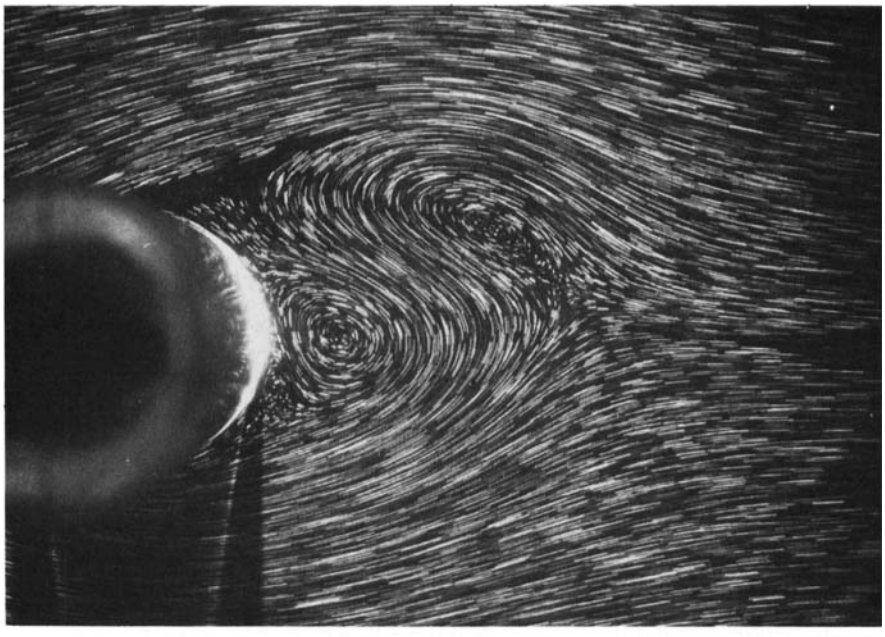

(*g*) $t^* = 3$

(*h*) $t^* = 3.5$

FIGURE 6(*g*,*h*). For caption see page 417.

(*i*) $t^* = 4$

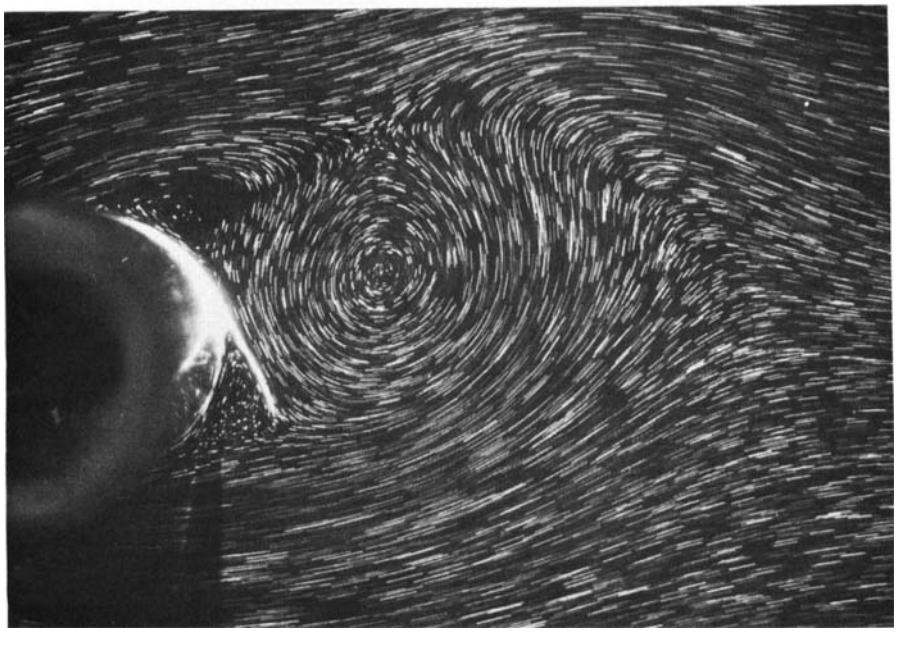

(*j*) $t^* = 4.5$

FIGURE 6(*i*,*j*). For caption see page 417.

(*k*) $\tau^* = 5$

(*l*) $t^* = 5.5$

FIGURE 6(*k*,*l*). For caption see facing page.

(*m*) $t^* = 6$

(*n*) $t^* = 6.5$

FIGURE 6. Flow visualization of the wake development behind an impulsively started translating and rotating circular cylinder for $Re = 200$ and $\alpha = 0.5$.

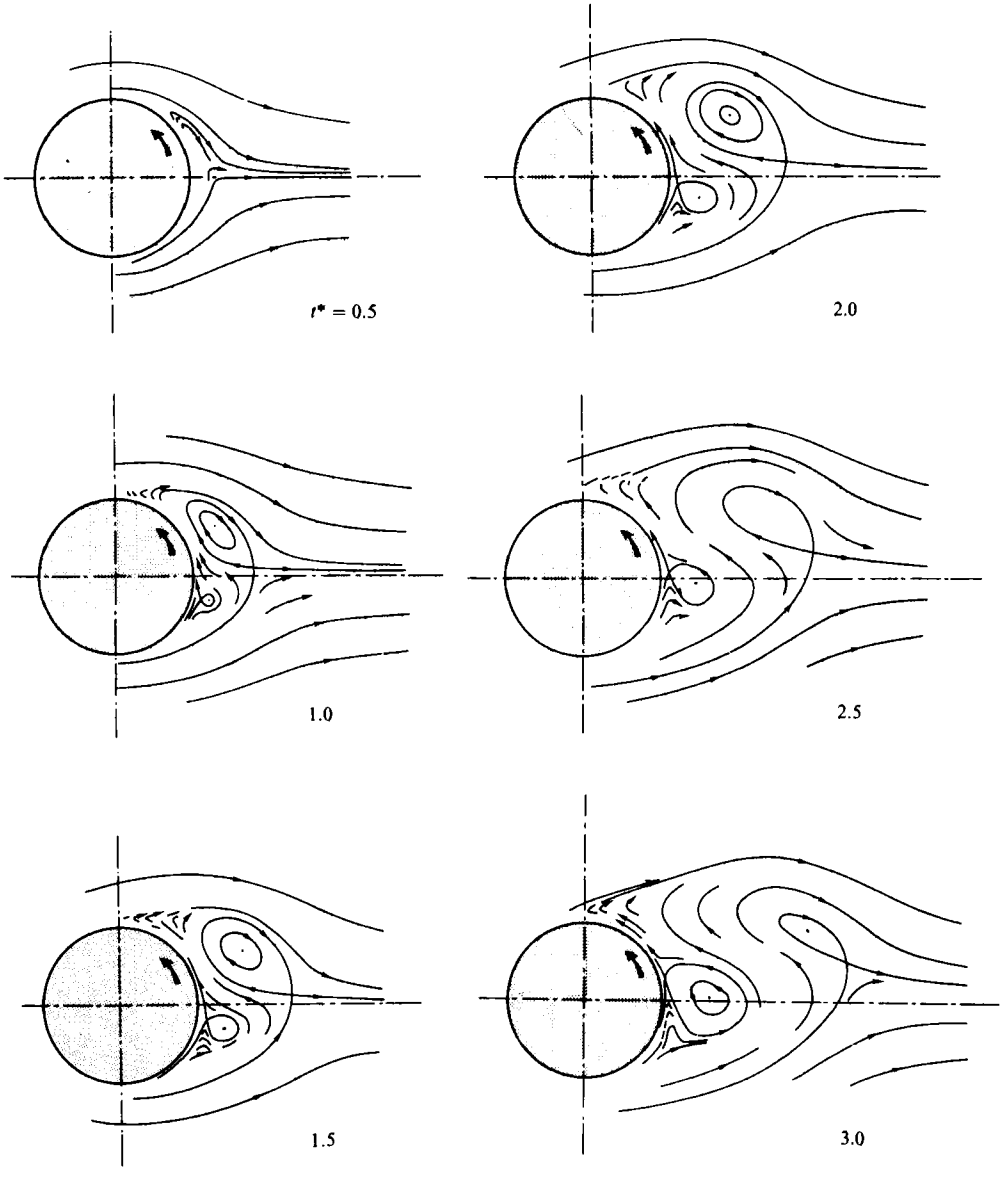

FIGURE 7. Part 1. For caption see facing page.

S_2 and S_3'.† All these features indicate that E_2 is beginning to disengage itself from the near wake. Simultaneously another eddy E_3'' is formed in the 'fluid wedge' below E_2. Afterwards E_2 is shed downstream in its turn and its size decreases. Then the two new eddies E_3' and E_3'' develop perpendicularly to the x-axis. They progress between the rotating layer and E_2 in such a way that they approach each other and finally coalesce (as described in §3), E_3' absorbing E_3'' to form the third eddy E_3. But, because the scaled time is limited to 4.5 when the 6 cm diameter cylinder is used,

† It might be thought that an intermediate configuration with a common boundary for E_2 and E_3', as proposed in the thesis of Ménard (1984), must occur; but because of its brevity it has not been possible to visualize this phenomenon.

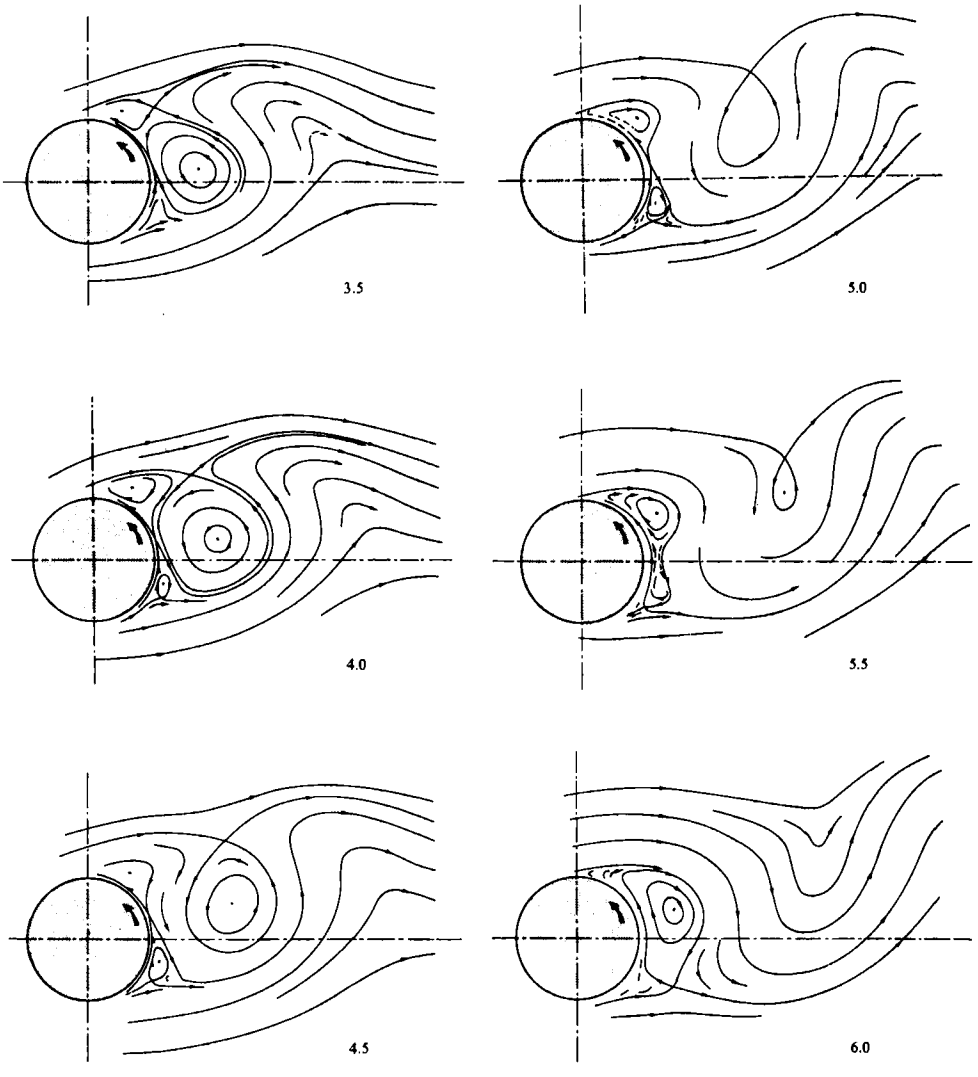

FIGURE 7. Time evolution of the streamline pattern behind an impulsively started rotating and translating circular cylinder for $Re = 200$ and $\alpha = 0.5$.

this last phase has insufficient time to take place. However, the phenomenon has been clearly observed with the 4 cm cylinder (figures 6*k–n*) which allows us to extend the observation time to 6.5. All the precise details observed in the experiments over the complete range of time appear also in the calculations of Badr & Dennis (1985).

5. Evolution of the time development of the wake flow pattern with the speed ratio α

The time development of the wake flow pattern having been presented in detail for $\alpha = 0.5$, we will now show briefly how the flow evolves when the speed ratio α varies, Re remaining fixed at 200. First, let us examine what happens when α decreases. In the period preceding the eddy shedding, the flow structure tends to become similar to that induced by a pure translation (i.e. $\alpha = 0$). In particular, the

asymmetry exhibited by the two eddies E_1 and E_2 becomes less and less marked. Thus, for $\alpha = 0.28$ (figure 8), which is the smallest value of α ($\alpha \neq 0$) studied in this work, and for $t^* < 2.5$, E_1 and E_2 grow similarly in size and in strength while having, however, the structure described previously, i.e. with S_1 and S_2 in opposite directions as represented in figure 5(*a*). From $t^* = 2.5$, E_1 is shed and E_2 increases rapidly, forcing the fluid to follow more and more distorted trajectories to pass around it. For $\alpha = 0.5$ this distortion was never as marked because, soon after E_1 was shed, it was possible for E_2 to be shed in its turn owing to the splitting of the 'fluid tongue' as explained in §4. Indeed this splitting phenomenon caused the formation of E_3' and consequently the freeing of E_2 from the rest of the wake. However, for $\alpha = 0.28$, E_2 continues to grow up to the last observation time, in this case up to $t^* = 4.5$, at which time E_2 appears to be enormous.

Secondly, let us consider the evolution of the flow when, on the other hand, α increases beyond 0.5. As examples we will present successively the cases of $\alpha = 1$, $\alpha = 2.07$ and $\alpha = 3.25$. The corresponding photographs and streamlines are given in figures 9–12. Compared with $\alpha = 0.5$, the essential difference is due to the fact that E_2 appears later. Thus for $\alpha = 1$, up to $t^* = 2.5$, only E_1 can be observed and in the place of E_2 the streamlines form a sort of hump which is more and more accentuated as t^* increases. But, from $t^* = 2.5$, E_1 is shed and then goes slowly downstream causing the hump to flatten out. At $t^* \cong 3$, E_2 appears almost simultaneously with E_3', as can be seen in figures 9 and 10. Although E_2 is then weaker, the flow configuration is analogous to that for $\alpha = 0.5$ just before the transposition phenomenon: E_2 is closed towards the cylinder wall, whereas E_3' is closed in the downstream direction. But very soon after, i.e. between $t^* = 3$ and 3.5, the transposition of S_2 and S_3' (already mentioned in the previous section) occurs and E_2 is shed. Next E_3' is stretched in the direction of E_3'', which is formed in the wedge for $t^* = 4$; then at $t^* \cong 5$ the two eddies coalesce. In this case the coalescing process has been clearly captured on the photographs with the 6 cm cylinder and is shown in figures 9(*e*) and (*f*) for $t^* = 4$ and 4.5. The new phenomena observed in this $\alpha = 1$ case are again paralleled almost exactly in the calculations of Badr & Dennis (1985).

For $\alpha = 2.07$ the phenomena evolve logically, see figures 11(*a*)–(*c*) and 12. In particular, in this case, E_2 does not form with closed streamlines. Indeed only E_1 is observed up to $t^* = 3$, at which time it appears to be shed downstream. At $t^* = 3.5$ E_3' appears but E_2 still remains indistinguishable; only a distortion of the streamlines can be observed from $t^* = 4$ at the rear of E_3'. However, from the analysis made in §8, it seems that this observed distortion of the streamlines could indicate the existence of a very weak and already shed E_2. It is to be recalled that, when $\alpha > 1$, such structures should induce an oscillating wake (Calamote 1984). Finally, for the greatest value of α considered in the present work, 3.25, no other eddy appears after the shedding of E_1 (figure 11*d*); this seems in agreement with the visualizations of Prandtl (Prandtl & Tietjens (1934), plates 8 and 11) and with the analysis of Calamote (1984) of the far wake, from which it appears that the Bénard–Kármán street is then completely destroyed.

In summary, it appears that the rotation strongly influences the near-wake formation, but mainly only the formation of the eddies E_i following the first one E_1. Thus E_2 becomes very weak as soon as α becomes greater than 1, i.e. when the wall speed becomes greater than the free stream, and no subsequent eddies occur after E_1 when α is greater than about 2 (i.e. when, at the start, the wall speed is everywhere greater than the fluid speed). In fact E_1 seems to be different. Indeed its birth, very soon after the start of the motion, in a zone of high vorticity, seems to show that

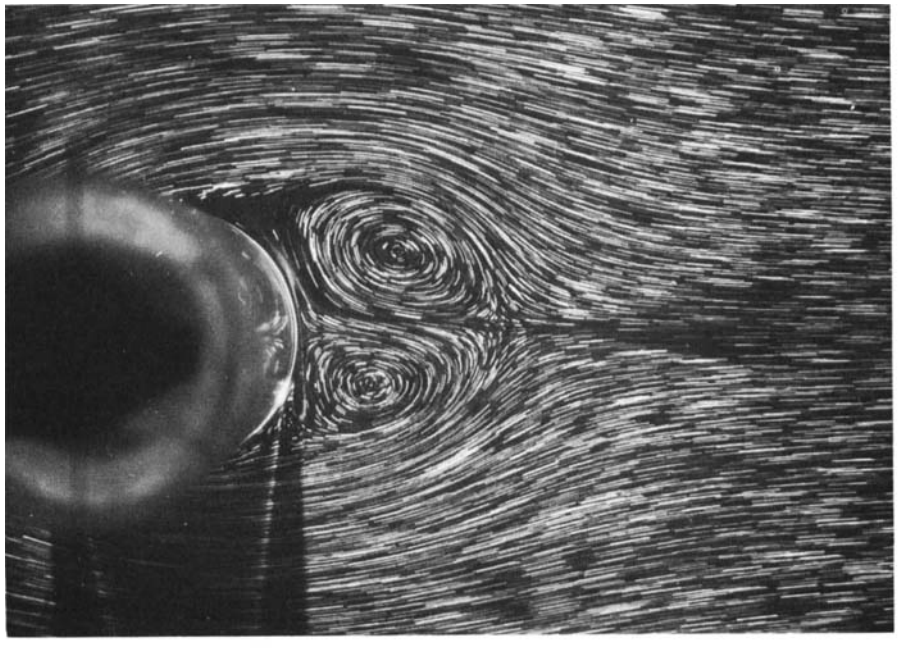

(*a*) $t^* = 2$

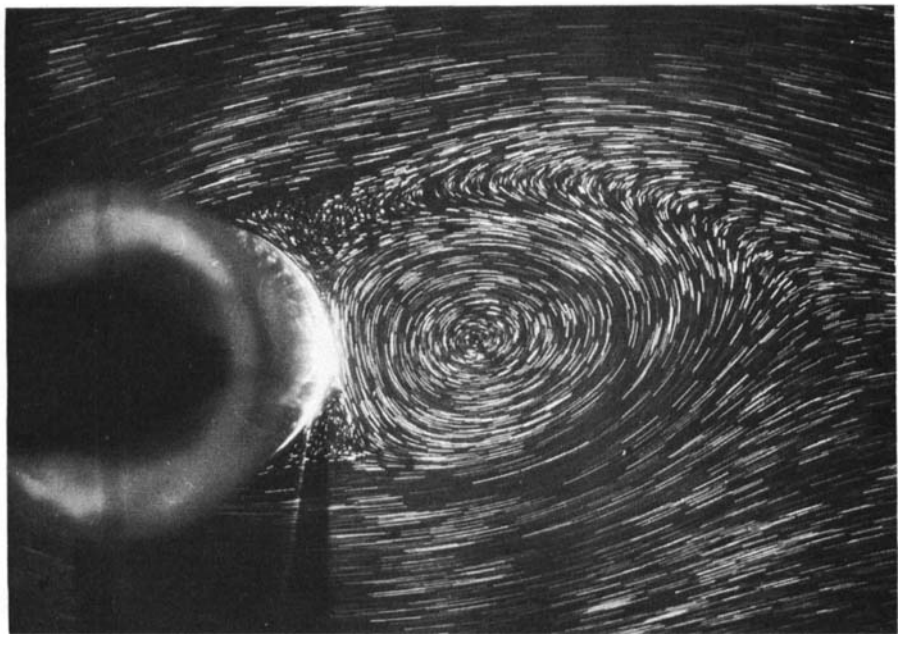

(*b*) $t^* = 4.5$

FIGURE 8. Visualizations of the wake development behind an impulsively started rotating and translating circular cylinder for $Re = 200$ and $\alpha = 0.28$.

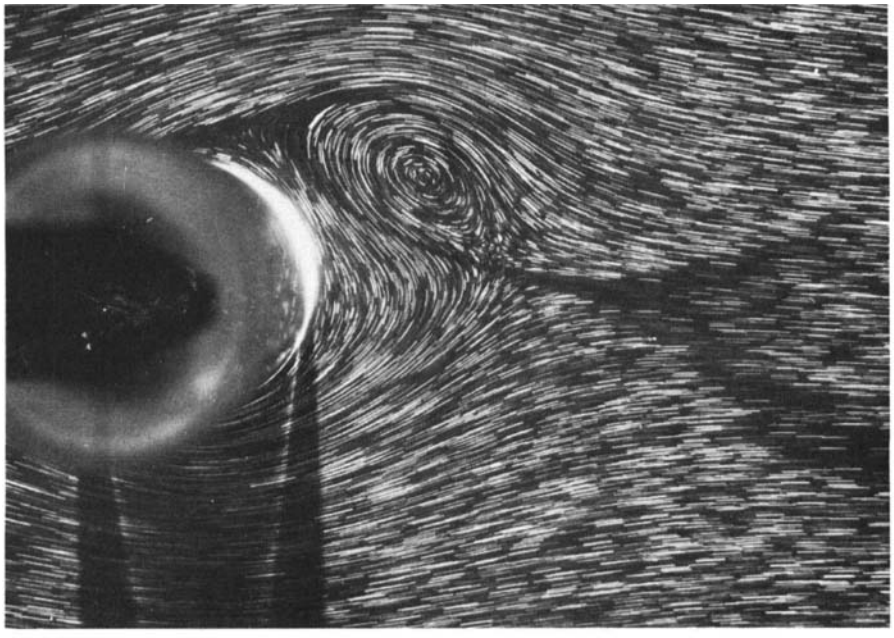

(*a*) $t^* = 2$

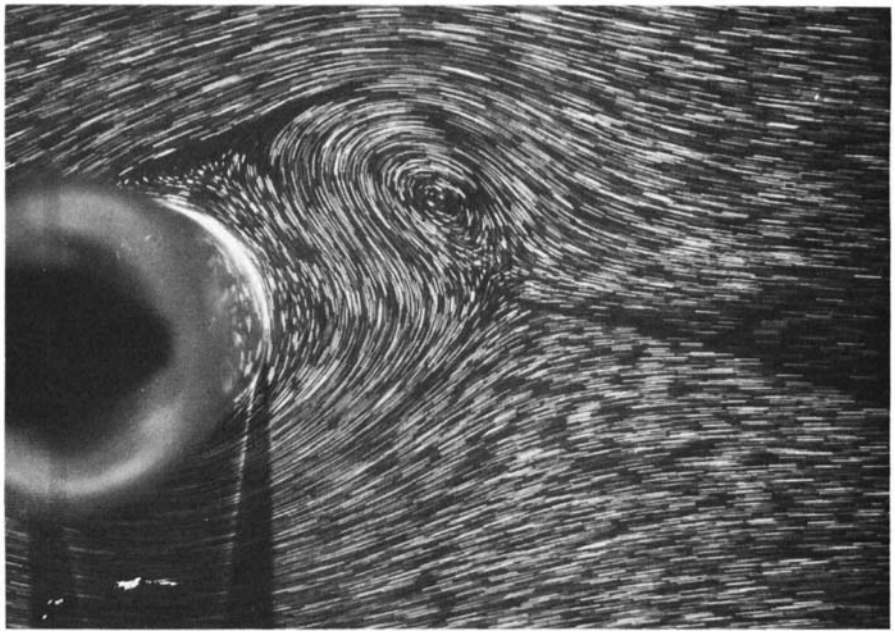

(*b*) $t^* = 2.5$

FIGURE 9(*a*,*b*). For caption see page 425.

(*c*) $t^* = 3$

(*d*) $t^* = 3.25$

FIGURE 9(*c*, *d*). For caption see page 425.

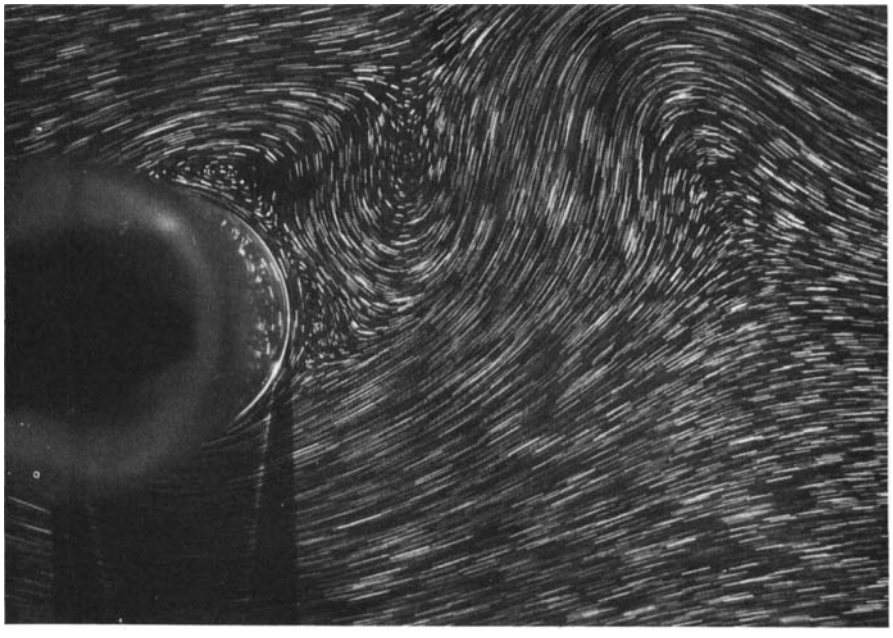

(*e*) $t^* = 4$

(*f*) $t^* = 4.5$

FIGURE 9(*e*, *f*). For caption see page 425.

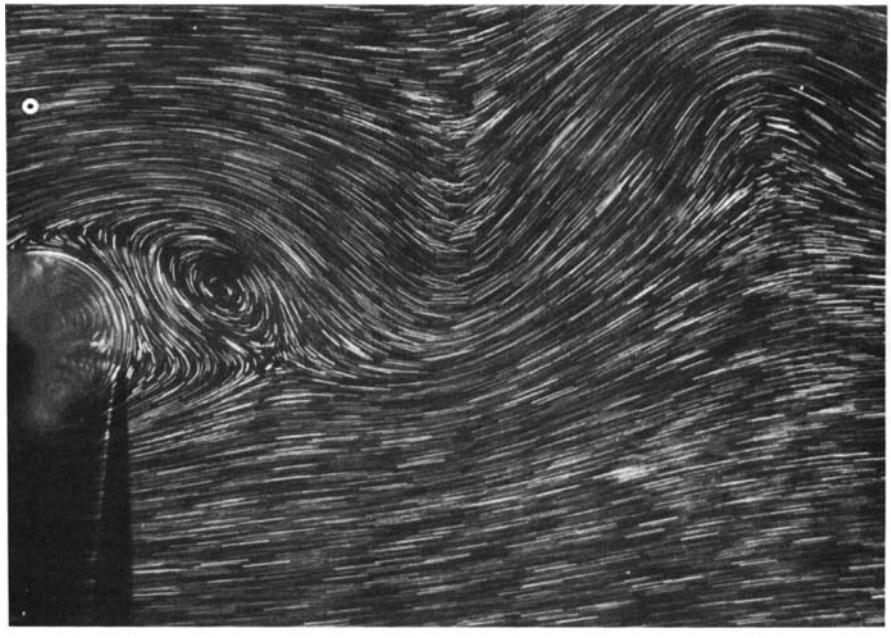

(*g*) $t^* = 6.5$

(*h*) $t^* = 7$

FIGURE 9. Visualizations of the wake development behind an impulsively started rotating and translating circular cylinder for $Re = 200$ and $\alpha = 1$.

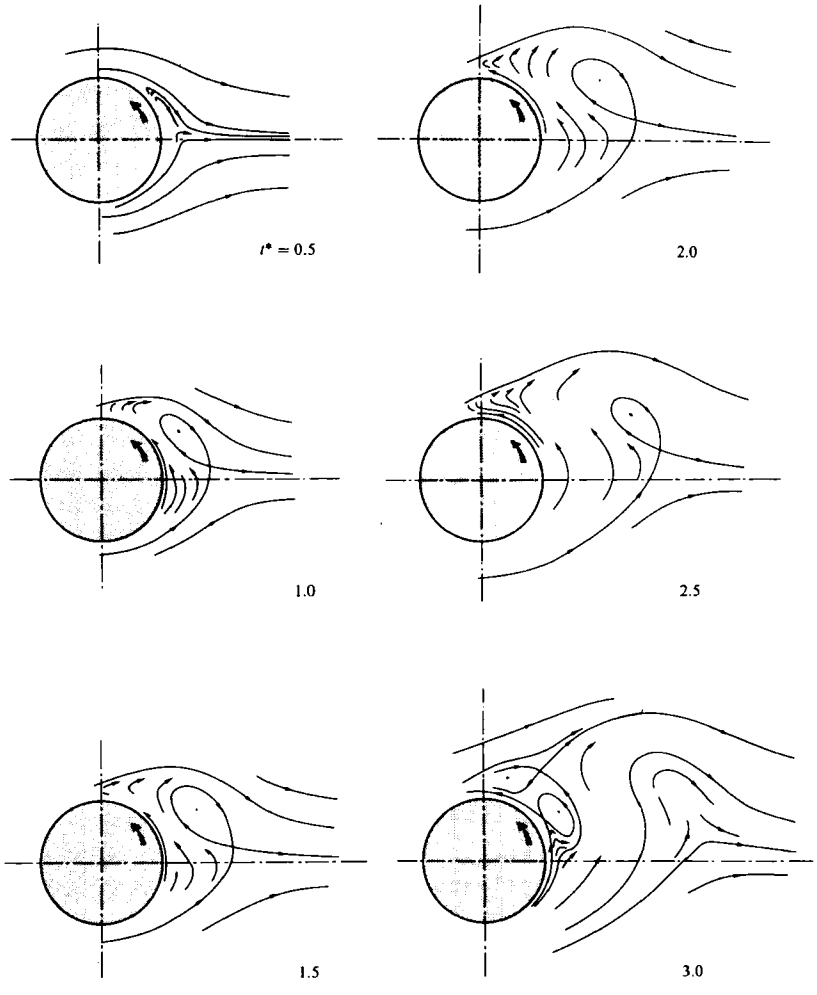

FIGURE 10. For caption see facing page.

it plays a role analogous to that of the starting vortex of an aerofoil. It contributes to the evacuation within the flow of the vorticity generated by the start of the motion.

In addition, although it has not been possible to prolong the study of the near-wake formation, it may be conjectured that, for low values of α ($\alpha < 1$), the process of formation of the last two eddies (E_2 and E_3) initiates the established regime: E_4, E_6, ... should form like E_2 whereas E_5, E_7, ... should be formed from the coalescence of two intermediate eddies like E_3.

6. Time evolution of certain flow properties

In order to illustrate precisely the flow configuration, we have determined the paths followed by the singular points of the flow (centre and saddle point of the eddies) during the wake formation. Moreover, we have measured the components u and v

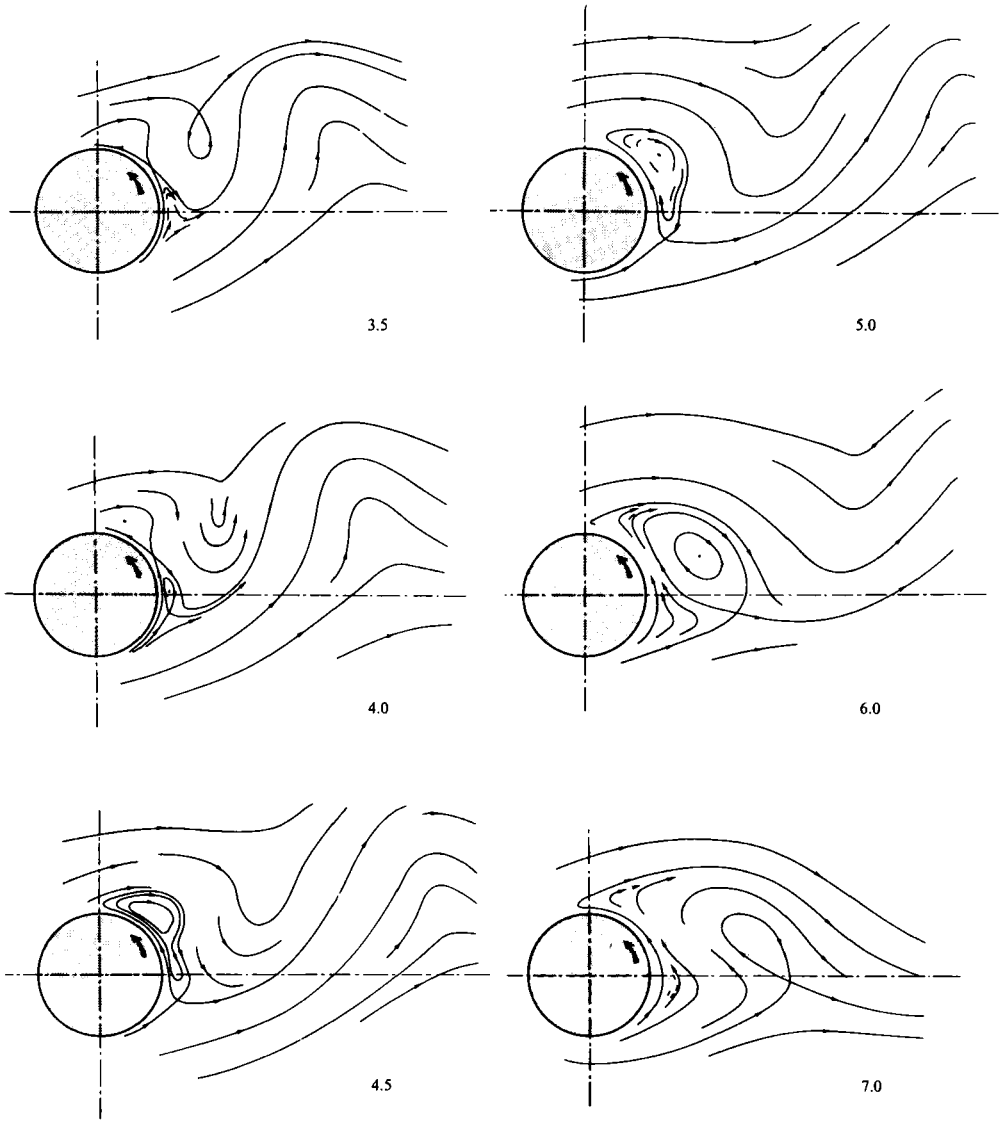

FIGURE 10. Time evolution of the streamline pattern behind an impulsively started rotating and translating circular cylinder for $Re = 200$ and $\alpha = 1$.

of the velocity of the particles and studied their distributions along the x- and y-axes (figure 4). This allows us to give their evolution with both time and the speed ratio α. These measurements have been made from the negative films, as mentioned in §2. More often than not the corresponding curves have been obtained from several pictures. So some dispersion of the experimental points may be observed in the more critical zone when the time evolution is very rapid. However, many of our results for the velocity distributions and the trajectories of the vortex centres and stagnation points are compared with results of calculations by Badr & Dennis (1985). The agreement is excellent.

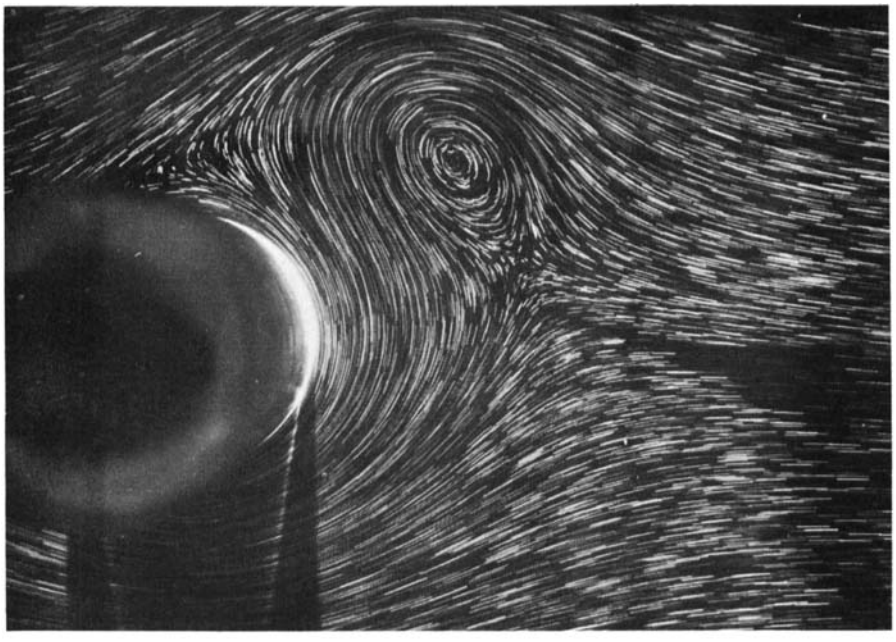

(*a*) $\alpha = 2.07$, $t^* = 2.5$

(*b*) $\alpha = 2.07$, $t^* = 3.5$

FIGURE 11 (*a*,*b*). For caption see facing page.

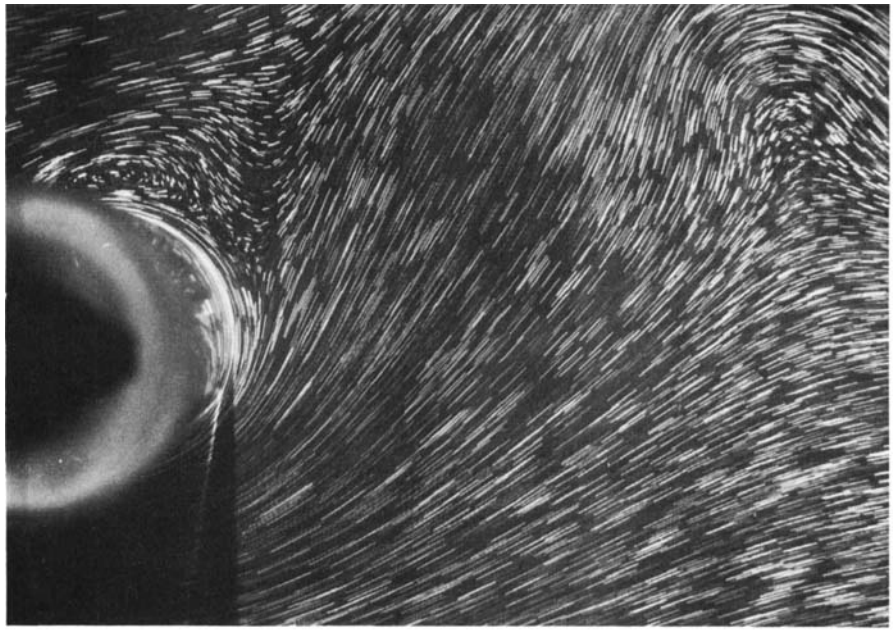

(*c*) $\alpha = 2.07$, $t^* = 4.5$

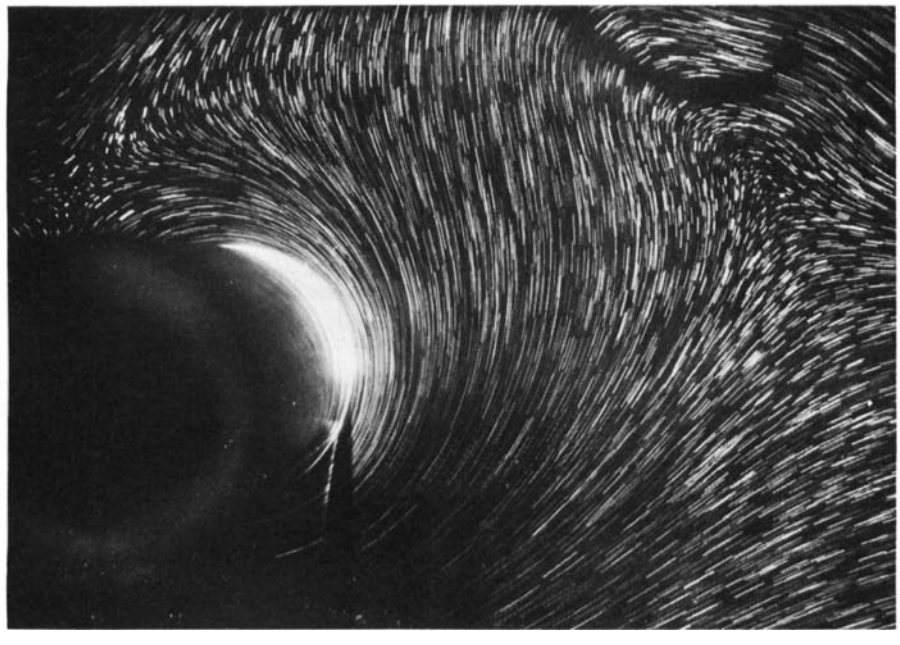

(*d*) $\alpha = 3.25$, $t^* = 4.5$

FIGURE 11. Visualizations of the wake development behind an impulsively started rotating and translating circular cylinder for $Re = 200$; $\alpha = 2.07$ and $\alpha = 3.25$.

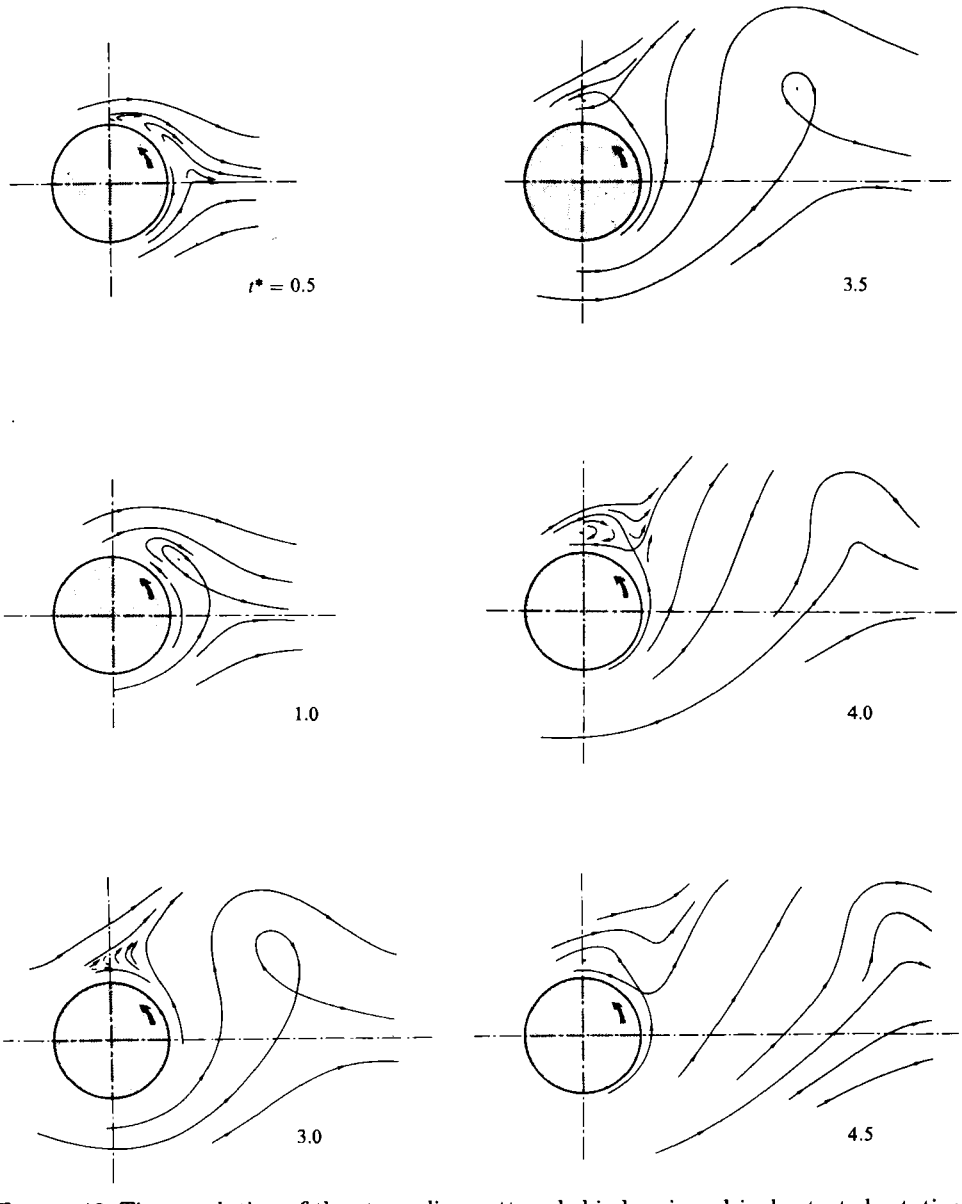

FIGURE 12. Time evolution of the streamline pattern behind an impulsively started rotating and translating circular cylinder for $Re = 200$ and $\alpha = 2.07$.

6.1. *Paths of the centre and closure point of the eddies*

The paths of the coupled points (C_1, S_1) of the eddy E_1 and, when they exist, those (C_2, S_2), (C_3', S_3'), (C_3'', S_3'') of E_2, E_3' and E_3'' have been determined for each of the speed ratios examined in this work; the curves relative to $\alpha = 0.5$ and $\alpha = 1$ are given as examples in figures 13(*a*) and (*b*), other results being given in the thesis of Ménard (1984). In addition the influence of the speed ratio α on the respective paths of C_1 and C_2 and on the time evolution of the characteristic length C_1S_1 of E_1 is shown in figures 14–16. Here we have collected together all the curves with that relative to $\alpha = 0$.

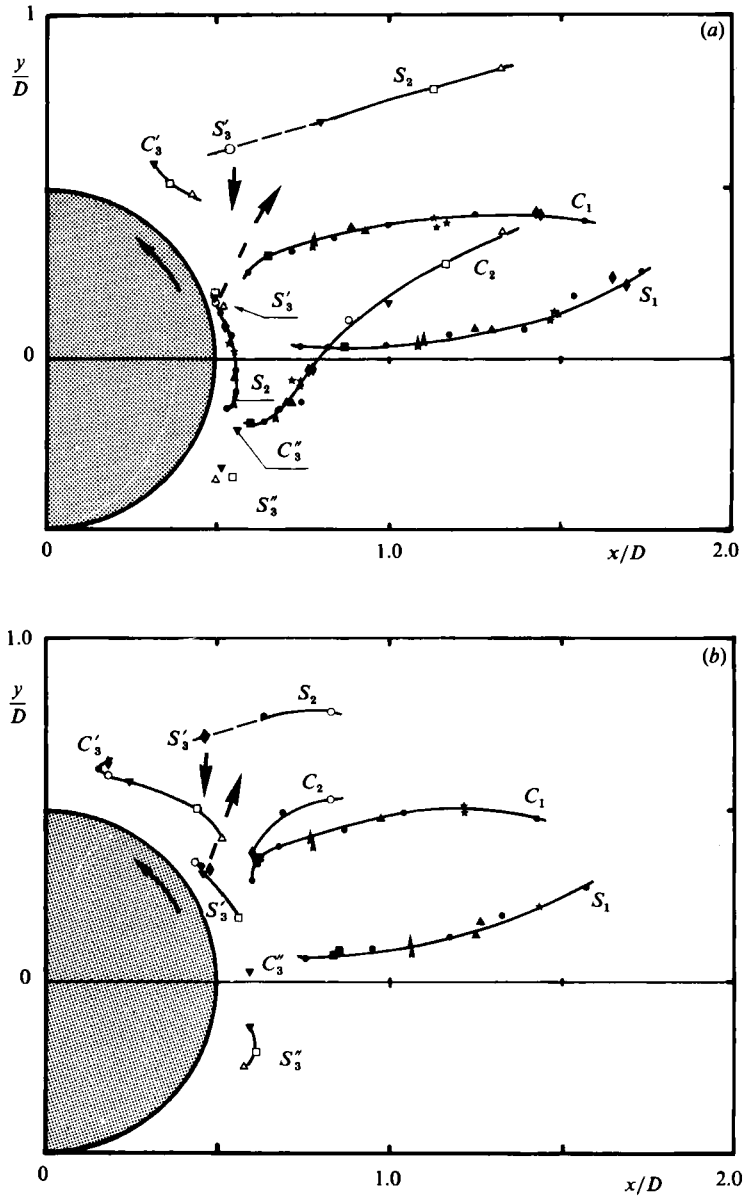

FIGURE 13. Paths of the centres C_i and the closure points S_i of the initial vortices T_i for $Re = 200$: ●, $t^* = 0.5$; ■, 1; ▲, 1.5; ▲, 2; ★, 2.5; ◆, 3; ○, 3.5; ▼, 4; □, 4.5; △, 5; •, intermediate values. (*a*) $\alpha = 0.5$, (*b*) $\alpha = 1$.

For each value of α it may be observed that both C_1 and S_1 pass downstream with time, whereas the behaviour of the pair (C_2, S_2), when they exist, is different. Indeed C_2 also passes downstream but S_2 moves up, along the rotating layer surrounding the cylinder, until the transposition (described in §§4 and 5) between S_3' and S_2 occurs, i.e. until E_2 starts to disengage itself from the near wake. Afterwards S_2 changes its initial direction, passing downstream in its turn.

Figure 14 shows that the paths of C_1 are further displaced above the x-axis as α increases. The particular behaviour of C_1 for $\alpha = 3.25$ when t^* increases beyond 3

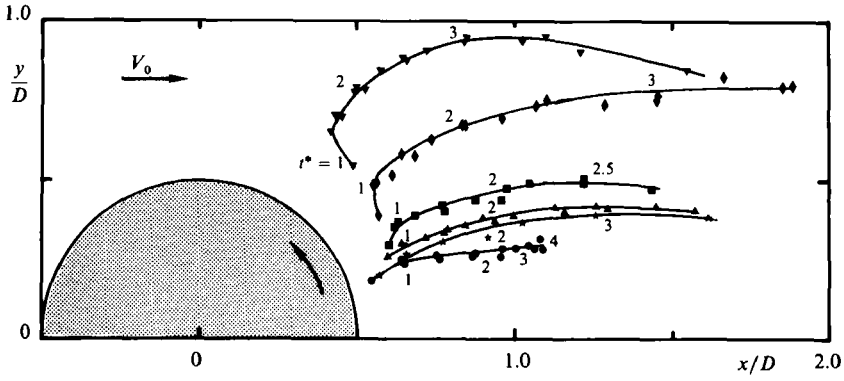

FIGURE 14. Evolution with α of the path of C_1: ●, $\alpha = 0$; ★, 0.28; ▲, 0.5; ■, 1; ◆, 2.07; ▼, 3.25.

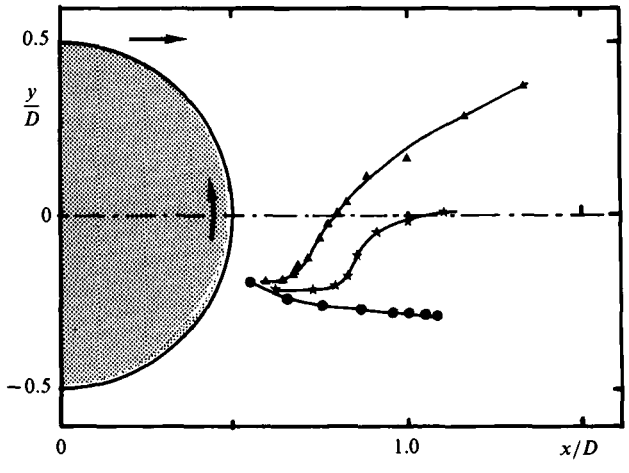

FIGURE 15. Evolution with α of the path of C_2: ●, $\alpha = 0$; ★, 0.28; ▲, 0.5.

(figure 14) is certainly due to the confining-wall effect which is equally well marked as α and t^* increase. Figure 16, which presents the time evolution of the length C_1S_1, gives an idea of the behaviour of the first eddy E_1; in particular, it should be recalled that (as explained in §3) the decrease of C_1S_1 is an indication of the detachment of E_1. On the figure it is seen that, except for the curve of $\alpha = 0$, which is a particular case because the eddies do not detach during the period of observation, all the other curves pass through a maximum at a certain time t^*_M. Two aspects of behaviour are noteworthy. First, for smaller values of α ($\alpha < 1$), t^*_M decreases when α increases; thus it decreases from about 2.5 to 1.75 when α increases from 0.28 to 1. Secondly, for larger values of α ($\alpha > 1$), t^*_M maintains a constant value of about 2.2. Likewise, the maximum of C_1S_1 itself decreases when α increases to 1 and then increases with α.

These two types of behaviour are due to the absence of a well-formed E_2 for $\alpha > 1$ and then, for the largest values of α, to the absence of any eddies after E_1.

It may also be noticed that, while the size of E_1 passes through a maximum, its saddle point S_1 moves up almost simultaneously from the x-axis. These combined features show that, although it is difficult to speak precisely about eddy shedding

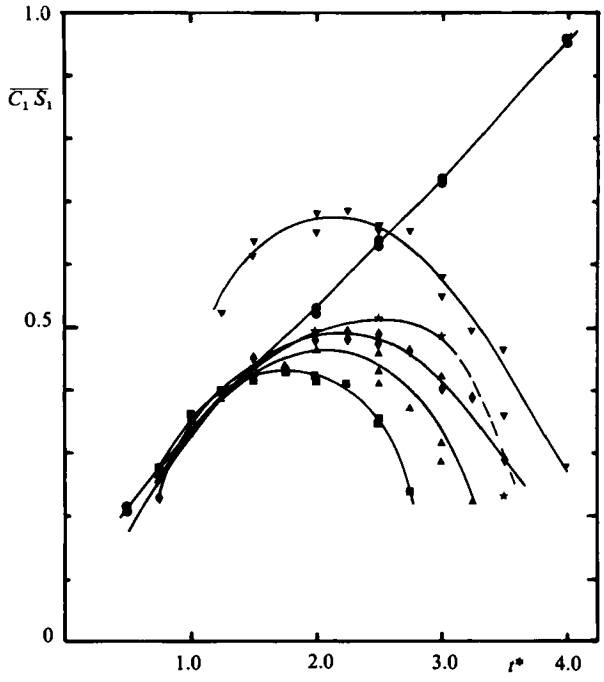

FIGURE 16. Comparison of the time evolution of the characteristic length $\overline{C_1 S_1}$ of E_1 for various values of α: ●, $\alpha = 0$; ★, 0.28; ▲, 0.5; ■, 1; ◆, 2.07; ▼, 3.25.

since the eddies have never been really attached to the body, the eddies disengage effectively from the near wake at a given time. As will be shown in the next section, this freeing of E_1 is also associated with a particular behaviour of the velocity field.

6.2. *Velocity distribution along the x-axis*

The time evolution of the u- and v-component distributions along the x-axis have been obtained for $\alpha = 0.5$, 1 and 2.07 (Ménard 1984). As examples figures 17 and 18 present those for $\alpha = 0.5$ and 1. It is to be noted that the points where $u = 0$ with $v \neq 0$, or $v = 0$ with $u \neq 0$, correspond respectively to either streamlines intersecting the x-axis perpendicularly or tangent to it. In all the cases studied positions of the u-curves are as expected from comparison with the one for the potential flow (without circulation) which has been added for comparison.

So let us first examine (figure 17*a*) the evolution of u along the flow axis at different times when $\alpha = 0.5$. It is seen that as time increases the curves move away from that for potential flow and, after $t^* > 0.5$, possess a region when the u-velocity component is negative, indicating a zone where the flow can be characterized as 'reversed' since this u-component is in the direction opposite to the free stream. In this region of reversed flow the magnitude of u passes through a maximum at a given distance from the cylinder. The value of this maximum increases up to $t^* = 2$ but, afterwards, it decreases. For example $|u|_{\max} = 0.42 V_0$; $0.64 V_0$ and $0.32 V_0$ for $t^* = 1.5$, 2 and 2.5 respectively. However, the length L of the part of the x-axis where u is negative continues to increase up to $t^* = 3$. Beyond this time u is always positive.

This time behaviour of the velocity distribution can be compared with that of the eddies. Thus it has been shown that E_1 may be characterized as shed after $t^* > 2$

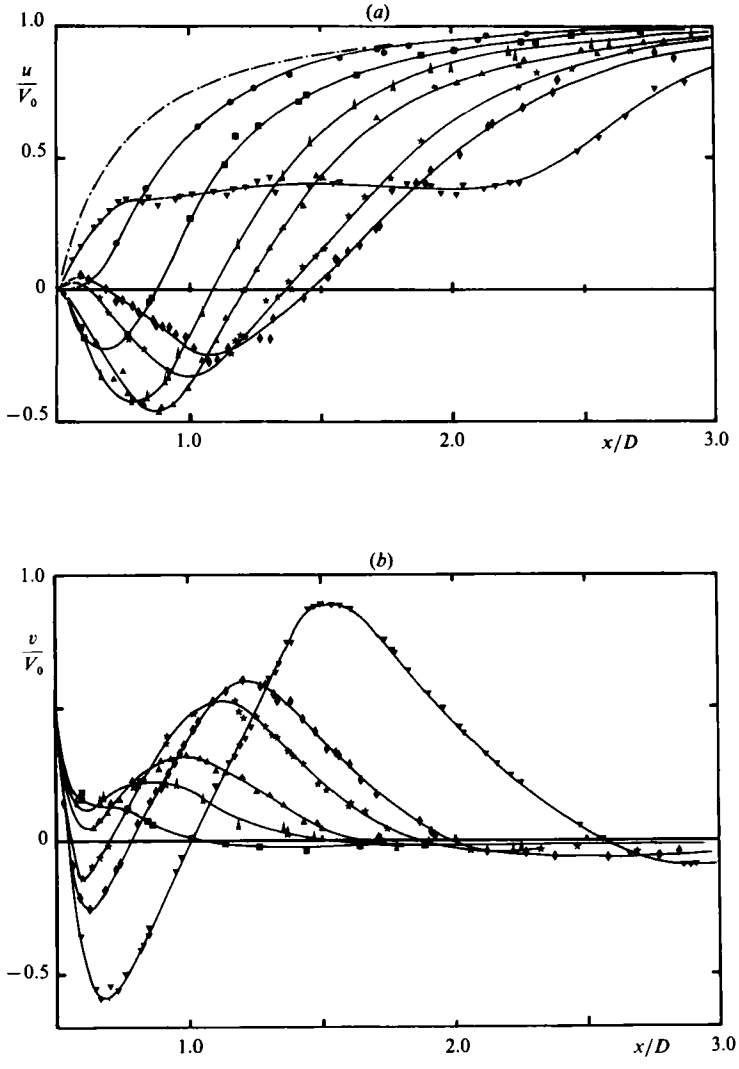

FIGURE 17. (*a*) Time evolution of the u-velocity-component distribution along the x-axis for $Re = 200$ and $\alpha = 0.5$: ●, $t^* = 0.5$; ■, 1; ▲, 1.5; ▲, 2; ★, 2.5; ◆, 3; ▼, 4; —·—, potential flow. (*b*) Time evolution of the v-velocity-component distribution along the x-axis for $Re = 200$ and $\alpha = 0.5$: ■, $t^* = 1$; ▲, 1.5; ▲, 2; ★, 2.5; ◆, 3; ▼, 4.

(figure 16) causing the fluid to have more space to circulate between the cylinder and itself and the velocities in the reversed flow to decrease. Further, for $t^* > 3$, the centre of E_2 passes clearly above the x-axis (figure 15) as E_2 is swept upwards by the rotation. It must be observed also that this upward motion of E_2 induces, from $t^* = 2.5$, positive values of u in the very near vicinity of the cylinder wall, indicating that the saddle point S_2 of E_2 has already crossed the x-axis and consequently, from this time, this axis intersects the fluid wedge described in §§4 and 5. At $t^* = 4$ E_2 is disengaging itself from the near wake and S_2 has been shifted to its upper part. So, along the x-axis, the flow is globally orientated in the direction of the free stream.

It may also be noted that, on their main positive part (i.e. outside the zone adjacent to the cylinder), the u-curves fit well with each other up to $t^* = 3$. When x is in-

creasing they tend towards the free-stream velocity V_0. This limit is reached less rapidly as time increases, indicating the increase with t^* of the extent of perturbation in the downstream direction. But, for $t^* = 4$, the curve differs radically from the previous ones: first, u increases rapidly when the x-axis passes through both the fluid wedge and the first part of E_2, and then it increases very slowly in the second part of E_2. Beyond E_2 u has an almost constant value of 0.4 up to a distance from the cylinder of about 1.8 times its diameter (i.e. at the level of E_1). It is at this stage only that the curve becomes similar to the others. A greater dispersion of the experimental points is observed at this time; it is owing to the rapid evolution of the flow structure. In particular, E_2 has just pivoted upwards to be shed.

The simultaneous behaviour of the v-component (figure 17*b*) is also strongly influenced by the development and the upwards motion of E_2. Thus the curves start from $v/V_0 = 0.5$ for $x/D = 0.5$ (i.e. on the cylinder wall) with a slope of about -10, after which they undulate before tending towards zero through negative values. The extrema of the curves, which are all the more marked as t^* increases, are effectively essentially induced by the evolution of E_2.

Figures 18(*a*) and (*b*), which present the u- and v-distributions for $\alpha = 1$, give some idea of the evolution with α. It may be noted in particular that the negative values of u decrease in magnitude; they will disappear for $\alpha = 2.07$. Likewise the minima of v decrease in magnitude, as opposed to the maxima, which increase.

6.3. *Velocity distribution along the y^+- and y^--axes*

In order to point out how the Magnus lift behaves with time, figures 19 and 20 present (for $\alpha = 0.5$) the distribution of the u-velocity component along the y^+-axis, i.e. along the upper part of the diametral plane P_D perpendicular to the free-stream direction and along the y^--axis, i.e. along the lower part of P_D. Once more, on each figure, the curve for potential flow (without circulation) has been added as a reference.

6.3.1. *Velocity along the y^+-axis*

Along the y^+-axis it is seen that, except in a thin layer adjacent to the cylinder where the velocity is in the same sense as the rotation, the velocity is in the free-stream direction, i.e. against the rotation. Thus, when the distance from the cylinder wall increases, u increases from $-\alpha V_0$ to a positive maximum value and then decreases towards V_0. Consequently, in contact with the wall there exists a zone where the u-component is negative. For $\alpha = 0.50$ the thickness e of this negative-u-layer increases with time, but remains very small, so that an important velocity gradient is induced. For example e increases from 0 to about $0.05D$ when t^* increases from 0 to 4; the corresponding non-dimensional velocity gradient $\partial u/\partial y$ is then greater than 10. Beyond this layer u increases up to a positive maximum which decreases with time but which is, in this case, always greater than V_0. For example $(u)_{max}$ decreases from $1.7V_0$ to $1.12V_0$ when t^* increases from 0.25 to 4; $(u)_{max}$ is $2V_0$ for the potential flow. The maximum value of u is reached at a distance which increases only slightly with time: it varies from about $0.15D$ for $t^* = 0.25$ to $0.3D$ for $t^* = 4$. So the velocity gradient remains high in this layer but then it decreases very rapidly when the distance from the cylinder wall increases.

We may notice also that, from $t^* = 2.5$, the maximum is no longer clearly marked: the last part of the curves are nearly parallel to the y-axis, showing that the extent of the perturbation caused by the cylinder is very great in this direction; it would be $50D$ for the inviscid flow with circulation if perturbations of the velocity lower than $0.01V_0$ were neglected. Furthermore it may be observed that the curves for $t^* = 3$

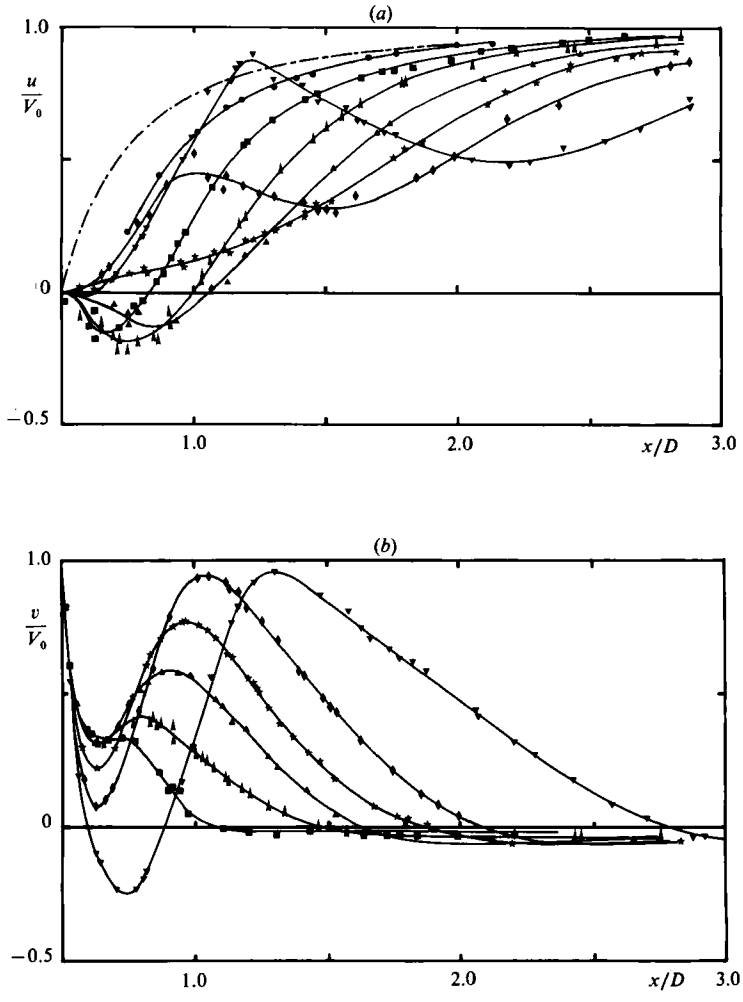

FIGURE 18. (*a*) Time evolution of the u-velocity-component distribution along the x-axis for $Re = 200$ and $\alpha = 1$: ●, $t^* = 0.5$; ■, 1; ▲, 1.5; ▲, 2; ★, 2.5; ◆, 3; ▼, 4; — · —, potential flow. (*b*) Time evolution of the v-velocity-component distribution along the x-axis for $Re = 200$ and $\alpha = 1$: ■, $t^* = 1$; , 1.5; ▲, 2; ★, 2.5; ◆, 3; ▼, 4.

and 4 are not much different; in particular they almost merge into a single curve in the zone where the velocity gradient is important, i.e. up to the distance from the cylinder wall of $0.2D$. The flow seems to be rapidly established in this zone as opposed to what happens along the flow axis where a very great change occurs between $t^* = 3$ and 4.

When α increases, the curves (Ménard 1984) are similar to those for $\alpha = 0.5$ during the earlier stage of the flow development and in the vicinity of the cylinder wall with, however, an increase of the thickness of the negative-u-layer. But, beyond a certain time, some clear differences appear: for example, the curves cease to fit as well as they do for $\alpha = 0.5$. Furthermore the u-component of velocity decreases when α increases, remaining even more consistently smaller than V_0 when $\alpha = 2.07$ and $t^* > 2.5$.

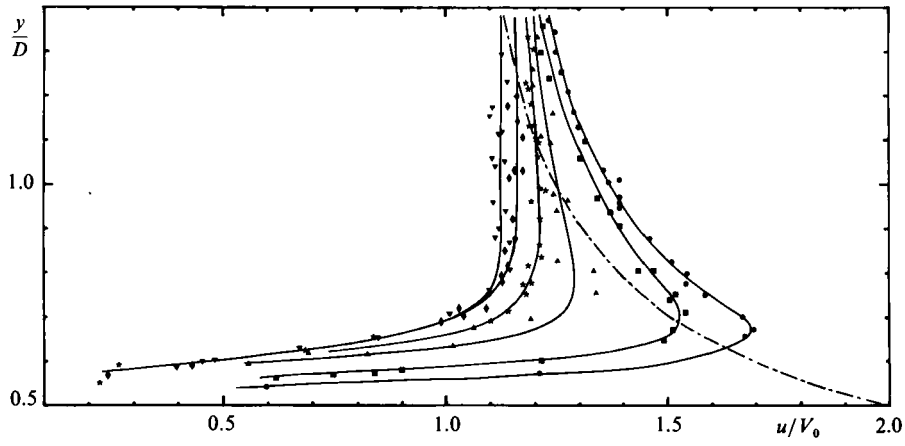

FIGURE 19. Time evolution of the u-velocity-component distribution along the y^+-axis for $Re = 200$ and $\alpha = 0.5$: ●, $t^* = 0.5$; ■, 1; ▲, 2; ★, 2.5; ◆, 3; ▼, 4; —·—, potential flow.

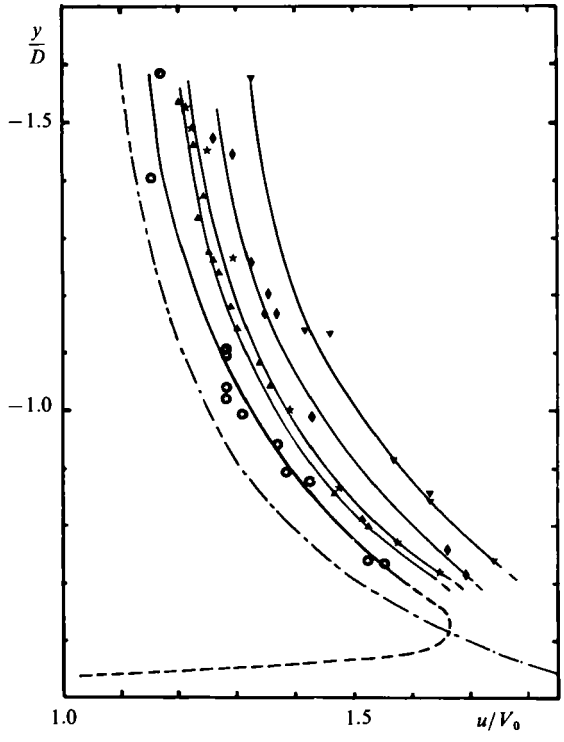

FIGURE 20. Time evolution of the u-velocity-component distribution along the y^+-axis for $Re = 200$ and $\alpha = 0.5$: ✪, $t^* = 0.25$; ▲, 2; ★, 2.5; ◆, 3; ▼, 4; —·—, potential flow.

6.3.2. *Velocity along the y^--axis*

Now, if we consider the velocity evolution along the y^--axis, it is seen that u increases rapidly in a thin layer of thickness probably about $0.2D$,† from αV_0 to a maximum and then decreases regularly towards V_0 going away from the cylinder; this u-maximum increases with time. As an example figure 20 shows the u-distributions for $\alpha = 0.5$ when the time increases to 4. It should be noticed that, beyond this layer of $0.2D$, the u-component is everywhere greater than the potential-flow velocity, contrary to the corresponding distributions along the y^+-axis for which the potential curve intersects with the other curves at a distance that increases rapidly with time, more so as α increases. After a given time the curves relative to the upper axis remain everywhere below the potential one. This comparison between the respective u-evolutions along the y^+- and y^--axes shows clearly that just after the start of the motion the velocity distributions are similar on the two parts of the y-axis and close to the potential-flow-velocity distribution. But, when time increases, the velocities decrease above the cylinder, whereas they increase below it, the distributions becoming, with increasing time, more and more asymmetrical. As explained in the introduction it is this velocity asymmetry, increasing with α which induces the Magnus lift.

7. On the flow structure in the neighbourhood of the front stagnation point

The determination of the flow pattern around the abruptly started rotating and translating cylinder has been completed by taking some photographs of the upstream region in order to determine the structure in the vicinity of the front stagnation point S (figure 5) and its time evolution. Some of these photographs are presented in figure 21 for $\alpha = 2.07$, and in figure 22 for $\alpha = 1$ and 3.25.

Very soon after the start of the motion the front stagnation point, initially at the intersection of the x-axis and the cylinder wall (figure 2), is abruptly shifted both in the direction opposite to the direction of the rotation and at a certain distance from the cylinder. This distance d increases with the speed α but does not vary much with time, at least for values of α up to 2. For example from $t^* = 1$ d is practically constant for $\alpha = 1$, being $0.05D$; for $\alpha = 2.07$ it is $0.05D$ at $t^* = 1$ and then is stabilized at $0.12D$. But, for $\alpha = 3.25$, d varies more with time, increasing from $0.1D$ to $0.4D$. The time variation of the angular location of S above the negative-x-axis also increases with α when t^* increases from 1 to 4; this variation ranges from about 43° to 49° for $\alpha = 1$, 35° to 46° for $\alpha = 2.07$ and 27° to 44° for $\alpha = 3.25$. The corresponding variation of θ is from 137° to 131°, from 145° to 134° and from 153° to 136°. The location of S is less rapidly established when α is greater; it is almost instantaneously established for values of α up to 1. The present results for the movement of this front stagnation point are found to be in excellent agreement with the calculations of Badr & Dennis (1985).

It may also be seen that, for the last observation time of $t^* = 4$, the angular location of S decreases only slightly with increase of α, whereas S moves clearly away from the cylinder. For the largest values of α, S will probably rotate further before the steady state is reached.

It may also be noticed that the upstream- and downstream-flow photographs

† The measurements were difficult in this region because of the presence of the shadow cast by the cylinder.

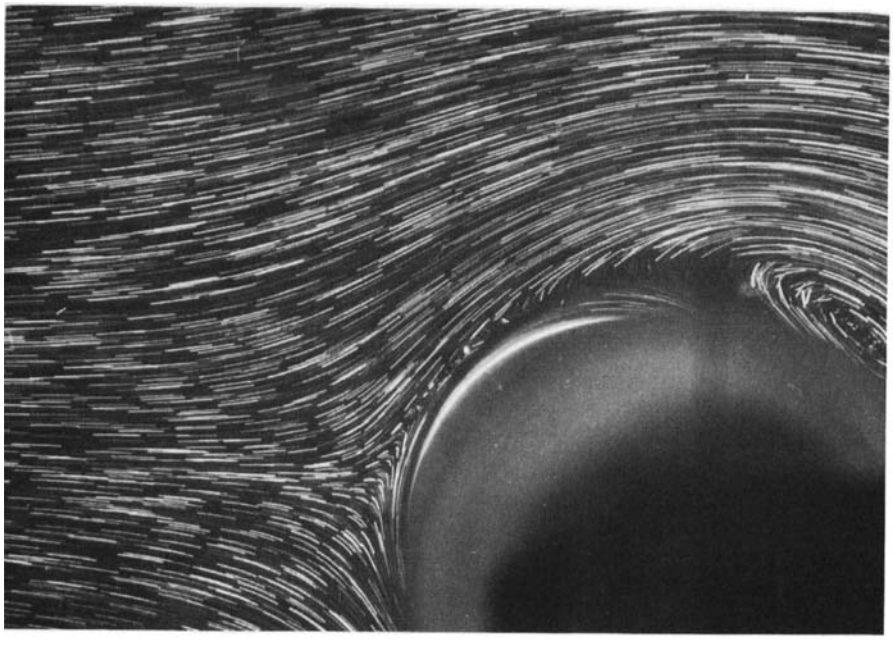

(*a*) $t^* = 1$

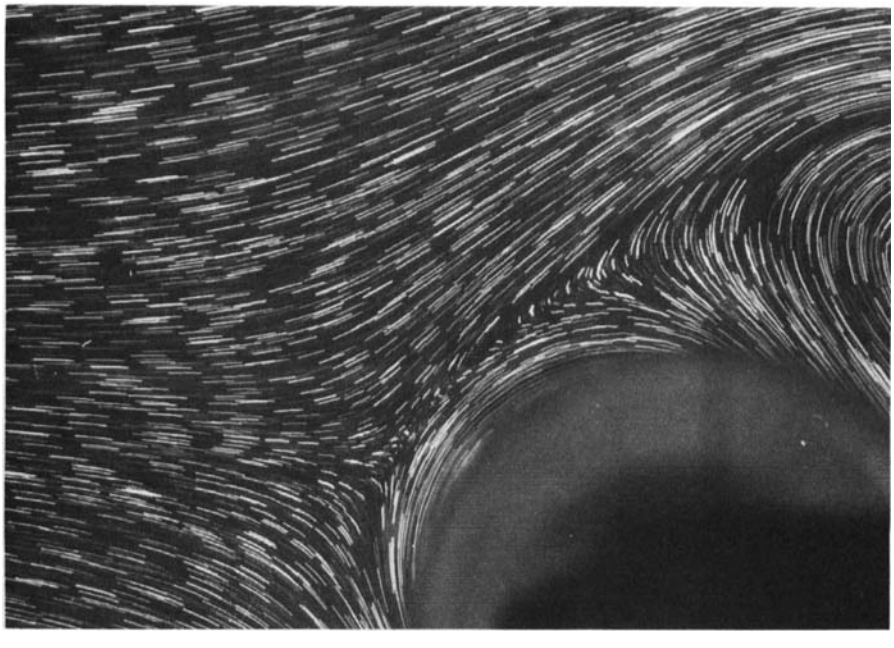

(*b*) $t^* = 2$

FIGURE 21 (*a*, *b*). For captions see page 440.

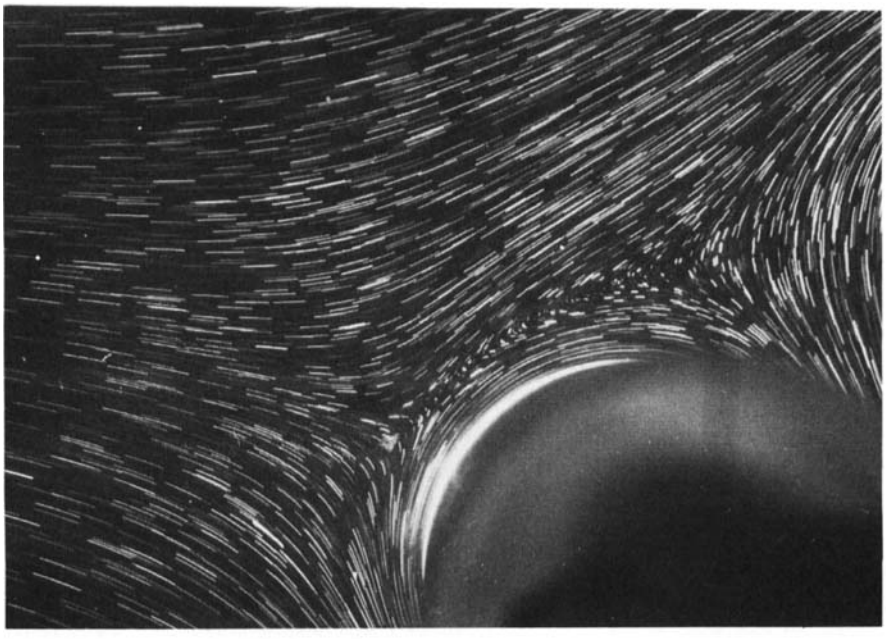

(*c*) $t^* = 3$

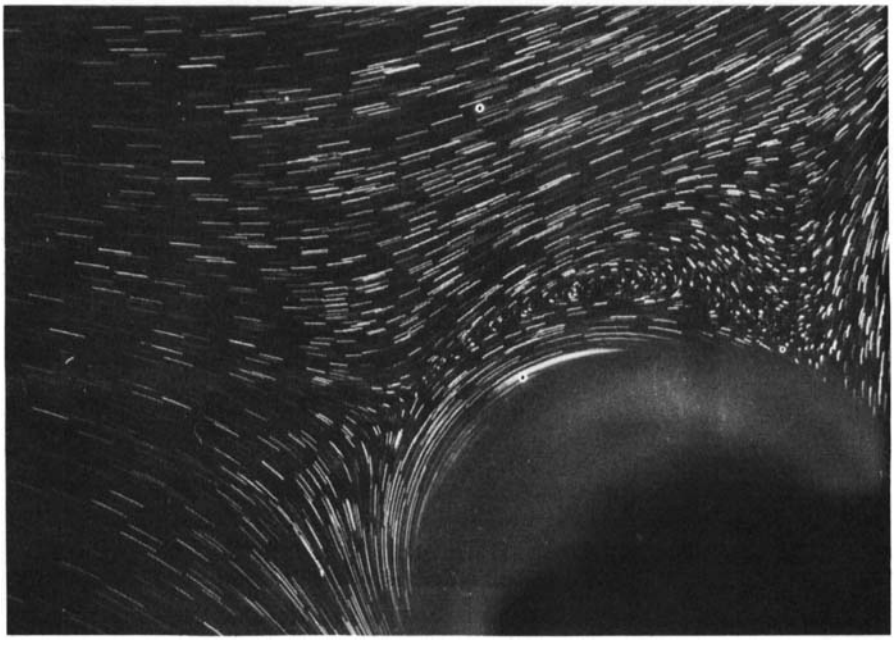

(*d*) $t^* = 4$

FIGURE 21. Visualizations of the flow development in front of an impulsively started translating and rotating cylinder for $Re = 200$ and $\alpha = 2.07$.

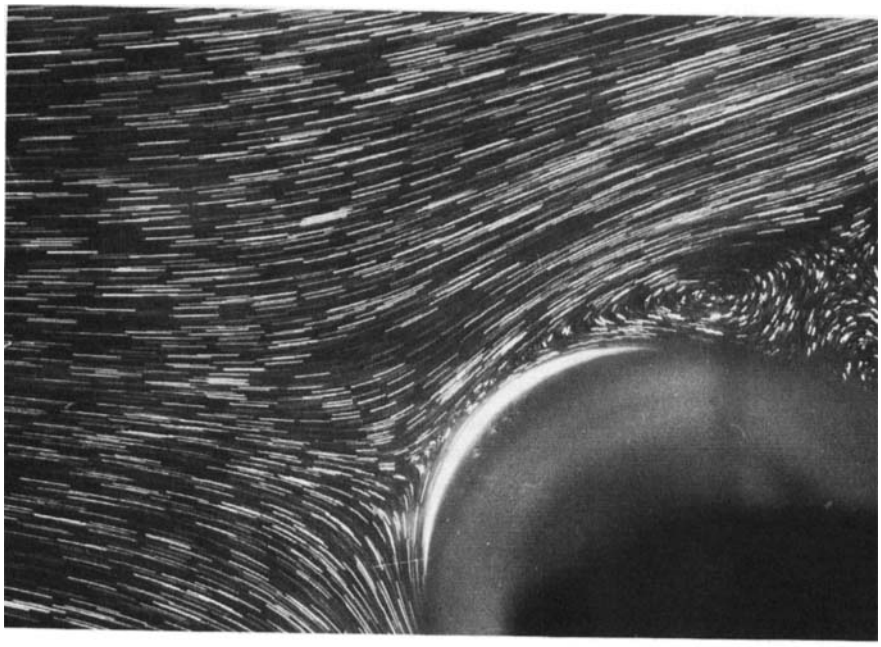

(*a*) $\alpha = 1, \quad t^* = 3$

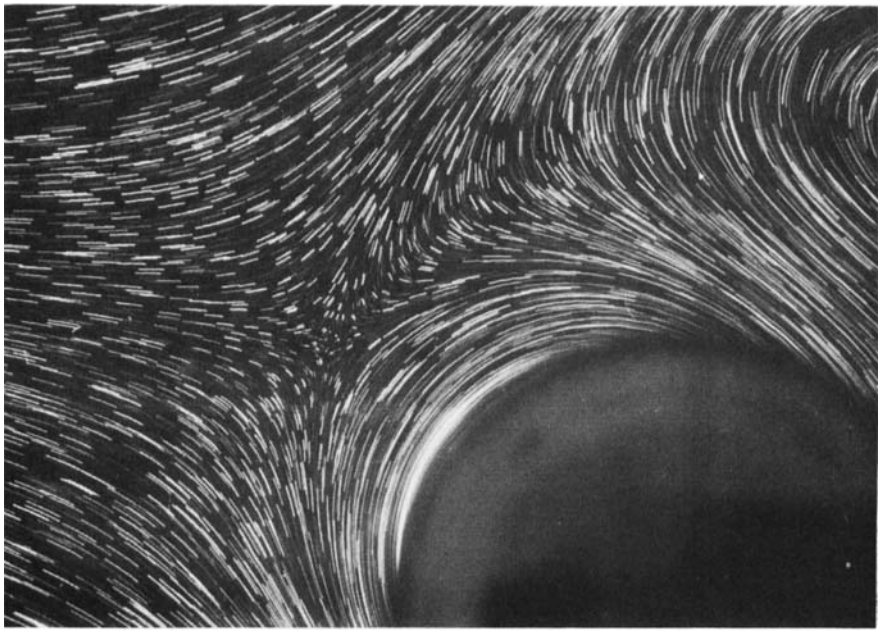

(*b*) $\alpha = 3.25, \quad t^* = 3$

FIGURE 22. Visualization of the flow development in front of an impulsively started translating and rotating cylinder for $Re = 200$.

present a common region: it is the one that corresponds to the left upper part of the wake. For example, for $\alpha = 2.07$, the part of the eddy that is seen in figure 21 is that of E_1 for the first three figures (a, b, c) and that of E_3' for the fourth (d). Consequently the two patterns can be connected and complete information can be deduced concerning the flow topology above the cylinder, i.e. along the upstream-moving wall which presents a point of particular interest as noticed by Koromilas & Telionis (1980).

8. Influence of Reynolds number on flow establishment

The influence of the Reynolds number on the flow establishment has been studied by considering, in addition to $Re = 200$, $Re = 500$ and 1000. It was found that globally the process of the wake formation as a function of α remains analogous to that observed for $Re = 200$. Thus two regimes have again been differentiated according to the formation or non-formation of alternate eddies after the first one E_1. But, when these alternate eddies exist, an intermediate phase has been observed which distinguishes three flow configurations corresponding to the behaviour of E_2: for a given Re and for values of α increasing progressively from zero these configurations are as follows:

E_2 occurs soon after the start of the motion in the lower part of the wake, develops, pivots upwards (by transposition of the saddle points S_2 and S_3'), detaches and persists in the wake, initiating an alternate-eddy street;

E_2 occurs a little later than before, still in the lower part of the near wake, but then, instead of developing regularly, it decreases and vanishes. However it recurs in the upper part of the wake only a short time before it pivots upwards, so only a short time before its detachment;

E_2 occurs directly in the upper part of the near wake, just before its detachment. The results of some calculations for $Re = 500$ which are in agreement with our present observations are given by Badr & Dennis (1985) and Badr *et al.* (1985).

The possible occurrence, vanishing and recurrence of E_2 show clearly that the rotation effects interact very little in the very early phase of the development, so that the separation may arise sufficiently upstream to permit the formation of E_2. After this, when these effects become more important, the boundary layer progresses downstream along the lower part of the cylinder, inducing dissolution of E_2. This delay in the interaction of the rotation effects becomes more marked as Re increases. More generally it has been observed that the relative influence of α decreases when Re increases. Thus when $Re = 200$, $\alpha = 0.5$ and 1 belong respectively to the first and third configurations, whereas, for $Re = 1000$, $\alpha = 1$ still belongs to the first configuration (although E_2 does not vanish for $Re = 1000$ when $\alpha = 1$, it increases, decreases and increases again before its detachment), $\alpha = 1.3$ to the second and $\alpha = 1.6$ to the third. Taking into account the observations of Calamote (1984) concerning the global far wake for $1000 < Re < 8000$, it may be thought that the last two configurations, which finally give rise to a weak eddy E_2 shed within the stream, will induce an oscillating wake rather than a well-formed alternate-eddy street. As to the limiting value of α beyond which any eddy is created after the first one, thus corresponding to the complete destruction of the eddy street, it seems to increase only very slightly with Re. In all cases this destruction has been observed when α becomes greater than about 2.

9. On the wall effects

Finally, a partial evaluation of the wall effect on the flow development has been made by varying the diameter of the cylinder (thus varying the wall-blockage ratio) and by comparing the trajectories of the characteristic points C_i, S_i of the initial eddies E_i that occur behind the rotating cylinder. Thus experiments have been conducted with two cylinders of 4 cm and 6 cm in diameter (as explained in §2), inducing a wall-blockage ratio λ (the ratio between the cylinder diameter and the transverse dimension of the tank) of 0.07 and 0.11 respectively. The observations were made for two speed ratios, $\alpha = 0.5$ and 1, with, in this study, the period of time limited to 4.5 (Ménard 1984). During this period no significant difference was detected when $Re = 200$ except for the transposition phenomenon of S_2 and S_3' which seems to occur a little later when the wall is nearer, the wake then being better stabilized. However, these wall effects interact effectively when $Re = 1000$ but without changing the global time evolution. Thus the eddies are a little more entrained by the rotation when they reside in the very near wake, whereas on the other hand the tank wall tends to push them towards the x-axis when they are shed within the stream and to accelerate their convective speed. On the whole, however, the results presented are clearly two-dimensional, as may be seen by comparison with the two-dimensional calculations of Badr & Dennis (1985).

9. Conclusion

By developing a special experimental apparatus which permits a quasi-instantaneous start, both into rotation and translation, of a circular cylinder in a quiescent liquid and by obtaining photographically the corresponding almost instantaneous velocity fields, we have gained new information on the mechanism of the near-wake development of this classical unsteady flow and shown the influence of the rotational effects. Indeed, the photographs complemented by the corresponding streamline patterns have allowed us to obtain details of the formation, evolution and detachment of the initial eddies E_i which appear in the near wake and to follow their behaviour both with the peripheral-to-translation-speed ratio α and with the Reynolds number; these results have been compared with those of the established regime. Furthermore a quantitative analysis of these pictures has provided the paths of the singular points (centre and closure point of the eddies) and the distributions of the velocity components along the flow axes.

The more important effects of the rotation are: (i) to induce a continuous fluid layer that rotates with the cylinder, so that the front stagnation point and the separation points are shifted from the wall within the stream. The thickness of this layer increases with α, but decreases when Re increases; (ii) to destroy the symmetry of the vorticity generated from the cylinder because of the difference between the relative fluid-to-wall velocity distributions on each side of the cylinder (one side moving as the free stream, the other moving against it) so that initial eddies with different size and strength are created; (iii) to accelerate the detachment of the eddies. For example, when $Re = 200$ (which has been chosen as a standard reference) and $\alpha = 0.5$, it has been shown that, during the period of observation which extends up to 7, three eddies (E_1, E_2, E_3) have time to form and to be shed downstream while, under the same conditions, for $\alpha = 0$ (i.e. for the pure translation) the wake would remain symmetrical and stably attached to the cylinder. The process of vorticity evacuation within the stream also seems to be modified, but the present experiments

do not permit us to be absolutely precise on this point. However, these experiments have brought interesting qualitative and quantitative information concerning the instantaneous velocity fields and streamline patterns. They help to serve as a guide in calculations, such as those which have been made in the parallel work of Badr & Dennis (1985).

Thus, concerning the formation of eddies, it has appeared that in all cases the first eddy E_1, whose behaviour has been found to be different from the subsequent ones, occurs just after the start of the motion and is shed within the stream at a time which varies only slightly with α and Re. On the other hand, the formation of the second eddy E_2 depends very much on α; its time of appearance increases and its size and strength decrease when α increases, until it manifestly disappears completely for α greater than a certain limiting value α_L. The value of α_L has been found to be not very dependent on the Reynolds number and to be about 2. For $\alpha > \alpha_L$ no other eddy is created after E_1 during the time of the observations, so that the eddy street must have been destroyed. An intermediate situation owing to the delay in the response of the fluid to the rotation has been demonstrated for α ranging from about 1 to α_L. Here E_2 is created but either it decreases and vanishes before appearing again on the upper side of the near wake just before its detachment, or it appears only just before its detachment. In each of these cases it is small and weak at the moment of shedding. Consequently the eddy street seems (from Calamote 1984) to have deteriorated into an oscillating wake.

New features have been detected in the processes of detachment of E_2 and of the formation of E_3. Thus E_2, when it exists, eventually turns towards the cylinder, pivots and disengages from the near wake by means of a transposition of its closure point with that of an intermediate eddy E_3', whereas E_3 comes from the coalescence of E_3' with another intermediate eddy E_3''. These phenomena must recur periodically, for respectively the even and odd eddies, but the period of observation of the present work has not been sufficient to confirm this.

The repercussions of these phenomena on the trajectories of the singular points and on the velocity distributions have been established. Thus it has been shown that the detachment of E_1 is revealed, at the same time, by the upwards displacement from the x-axis of its closure point S_1, by the decrease of its size, by the upwards motion of E_2 that passes through the x-axis and then by its rapid development. But it is also signalled by the clear decreases in the maxima of the negative-u-velocity-component distribution along the x-axis and of the positive-u-velocity-component distribution along the upper y-axis. Furthermore, it was found that the increase of Reynolds number from 200 to 1000 does not change the global structure of the near wake. However, the relative influence of the rotation is smaller and its effect is delayed; in addition, new phenomena of secondary-eddy formation and saddle-point transpositions occur.

Finally, the excellent agreement between these results and the numerical ones of Badr & Dennis confirm their respective validity. These results should be capable of providing some elements which may lead to a better understanding of unsteady flows over moving walls.

The authors have very much appreciated the collaboration with Professor S. C. R. Dennis and H. M. Badr, and wish to thank J. R. Defouge for his help in improving the English text.

REFERENCES

BADR, H. M. & DENNIS, S. C. R. 1985 Time-dependent viscous flow past an impulsively started rotating and translating circular cylinder. *J. Fluid Mech.* **158**, 447–488.

BADR, H. M., COUTANCEAU, M., DENNIS, S. C. R. & MÉNARD, C. 1985 Sur un comparaison des calculs numériques et des visualisations de l'écoulement d'un fluide visqueux, engendré par un cylindre en translation et en rotation. *C. R. Acad. Sci. Paris, t.* **300**, II, no. 12, 529–533.

BATCHELOR, G. K. 1967 *An Introduction to Fluid Dynamics.* Cambridge University Press.

BICKLEY, W. G. 1928 The influence of vortices upon the resistance experienced by solids moving through a liquid. *Proc. R. Soc. Lond.* A **119**, 146–156.

BOUARD, R. 1983 Etude de l'écoulement autour d'un cylindre soumis à une translation uniforme après un départ impulsif pour des nombres de Reynolds allant de 0 à 10^4. Thèse de Doctorat d'Etat de l'Université de Poitiers.

BOUARD, R. & COUTANCEAU, M. 1980 The early stage of development of the wake behind an impulsively started cylinder for $40 < Re < 10^4$. *J. Fluid Mech.* **101**, 583–607.

CALAMOTE, J. 1984 Effets de la rotation sur le sillage de cylindres tournants. Thèse de 3ème cycle de l'Université Aix-Marseille II.

CHARRIER, B. 1979 Etude théorique et expérimentale de l'effet 'Magnus' destiné à la propulsion éolienne de navires. Thèse de 3ème cycle de l'Université de Paris VI.

COUTANCEAU, M. & BOUARD, R. 1977*a* Experimental determination of the main features of the viscous flow in the wake of a circular cylinder in uniform translation. Part 1. Steady flow. *J. Fluid Mech.* **79**, 231–256.

COUTANCEAU, M. & BOUARD, R. 1977*b* Experimental determination of the main features of the viscous flow in the wake of a circular cylinder in uniform translation. Part 2. Unsteady flow. *J. Fluid Mech.* **79**, 257–272.

DIAZ, F., GAVALDÀ, J., KAWALL, J. G., KEFFER, J. K. & GIRALT, F. 1983 Vortex shedding from a spinning cylinder. *Phys. Fluids* **26**, 3454–3460.

GLAUERT, M. B. 1957*a* A boundary layer theorem, with application to rotating cylinders. *J. Fluid Mech.* **2**, 89–99.

GLAUERT, M. B. 1957*b* The flow past a rapidly rotating cylinder. *Proc. R. Soc. Lond.* A **242**, 108–115.

GUSTAFSON, T. 1933 On the Magnus effect according to the asymptotic hydrodynamic theory. *Hakan Ohlssons Buchdruckerei, Lund (Sweden)* (transl. *NACA* N-25921, 1954).

HONJI, H. & TANEDA, S. 1969 Unsteady flow past a circular cylinder. *J. Phys. Soc. Japan* **27**, 1668–1677.

INGHAM, D. B. 1983 Steady flow past a rotating cylinder. *Computers and Fluids* **11**, 351–366.

KOROMILAS, C. A. & TELIONIS, D. P. 1980 Unsteady laminar separation: an experimental study. *J. Fluid Mech.* **97**, 347–384.

KRHAN, E. 1955 The laminar boundary layer on a rotating cylinder in cross flow. *NAVORD Rep.* 4022, *Aerobal. Res. Rep.* 288, U.S., NOL. Maryland.

LUGT, H. J. 1979 The dilemma of defining a vortex. In *Recent Development of Theoretical and Experimental Fluid Mechanics*, pp. 309–321. Springer-Verlag.

MEHTA, U. B. & LAVAN, Z. 1975 Starting vortex, separation bubbles and stall: a numerical study of laminar unsteady flow around an airfoil. *J. Fluid Mech.* **67**, 227–256.

MÉNARD, C. 1984 Thèse de 3ème cycle de l'Université de Poitiers.

MOORE, D. W. 1957 The flow past a rapidly rotating cylinder in a uniform stream. *J. Fluid Mech.* **2**, 541–550.

O'BRIEN, V. 1981 Stagnation regions of separation. *Phys. Fluids* **24**, 1005–1009.

PERRY, A. E., CHONG, M. S. & TIM, T. T. 1982 The vortex-shedding process behind two-dimensional bluff bodies. *J. Fluid Mech.* **116**, 77–90.

PRANDTL, L. & TIETJENS, O. G. 1934 *Applied Hydro- and Aeromechanics* (transl. J. P. Den Hartog 1957). Dover.

RINALDO, A. & GIORGINI, A. 1983 A mixed discrete Fourier transform–finite difference algorithm for the solution of the Navier–Stokes equations. *Rep. no. CE – HSE – 83 – 13.* Perdue Univ., West Lafayette, Indiana.

SWANSON, W. M. 1961 The Magnus effect: a summary of investigation to date. *Trans. ASME* D: *J. Basic Engng* 461–470.

TANEDA, S. 1977 Visual study of unsteady separated flows around bodies. *Prog. Aero. Sci.* **17**, 287–348.

TANEDA, S. 1980 Visualization of unsteady flow separation. In *Flow visualization II* (ed. W. Merzkirch), pp. 253–257. Hemisphere.

TA PHUOC LOC 1975 Etude numerique de l'écoulement d'un fluide visqueux incompressible autour d'un cylindre fixe ou en rotation. Effet Magnus. *J. Méc.* **14**, 109–133.

TA PHUOC LOC 1980 Numerical analysis of unsteady secondary vortices generated by an impulsively started circular cylinder. *J. Fluid Mech.* **110**, 111–128.

TOWNSEND, P. 1980 A numerical simulation of newtonian and visco-elastic flow past stationary and rotating cylinders. *J. Non-Newtonian Fluid Mech.* **6**, 219–243.

WERLÉ, H. 1984 Visualisation hydrodynamique de l'écoulement autour d'un cylindre profilé avec aspiration, maquette de la turbovoile Cousteau-Malavard. *La Recherche Aérospatiale* **4**, 265–274.

WOOD, W. W. 1957 Boundary layers whose streamlines are closed. *J. Fluid Mech.* **2**, 77–87.